

Reach-Avoid Control Synthesis for a Quadrotor UAV with Formal Safety Guarantees

Mohamed Serry, Haocheng Chang, and Jun Liu

Abstract—Reach-avoid specifications are one of the most common tasks in autonomous aerial vehicle (UAV) applications. Despite the intensive research and development associated with control of aerial vehicles, generating feasible trajectories through complex environments and tracking them with formal safety guarantees remain challenging. In this paper, we propose a control framework for a quadrotor UAV that enables accomplishing reach-avoid tasks with formal safety guarantees. That is, our method yields a desired (position) trajectory to be tracked and an initial set, with respect to the quadrotor’s dynamics, such that for any point in that initial set, the resulting quadrotor position follows the desired trajectory and reaches the target safely while avoiding obstacles, where velocity and thrust safety bounds are satisfied. In this proposed framework, we integrate geometric control theory for tracking and polynomial trajectory generation using Bézier curves, where tracking errors are accounted for in the trajectory synthesis process. To estimate the tracking errors, we revisit the stability analysis of the closed-loop quadrotor system, when geometric control is implemented. We show that the tracking error dynamics exhibit local exponential stability when geometric control is implemented with any positive control gains, and we derive tight uniform bounds of the tracking error. We also introduce sufficient conditions to be imposed on the desired trajectory utilizing the derived uniform bounds to ensure the well-definedness of the closed-loop system. For the trajectory synthesis, we present an efficient algorithm that enables constructing a safe tube by means of sampling-based planning and safe hyper-rectangular set computations. Then, we compute the trajectory, given as a piecewise continuous Bézier curve, through the safe tube, where a heuristic efficient approach that utilizes iterative linear programming is employed. We present extensive numerical simulations with a cluttered environment to illustrate the effectiveness of the proposed framework in reach-avoid planning scenarios.

I. INTRODUCTION

Quadrotor UAVs have been a focal point in control theory due to their utilities in a wide variety of applications that involve surveying and delivering [1]. One of the main tasks concerning quadrotor applications is reaching specific target(s) while avoiding obstacles, which necessitates adopting and developing safe path planning and control algorithms for quadrotor UAVs. Standard approaches in the literature rely on constructing piecewise-continuous polynomial trajectories and then utilizing the differential flatness of quadrotor UAVs to derive controllers that can track the generated trajectories [2]. The generated trajectories are typically constructed by connecting waypoints using polynomial interpolants. The waypoints, which lay in the three-dimensional operating domain of the quadrotors, can be generated by sampling-based (e.g., RRT [3]), or node-based (e.g., A* [4]) methods. Besides reach-avoid problems, waypoints can also be obtained for more complex specifications such as temporal logic specifications [5]. For polynomial interpolation, standard polynomials

[2] or Bernstein polynomials [6] can be employed and desired trajectories are often obtained by solving nonlinear optimization problems. Various control approaches can then be employed to track the generated trajectories, including linearization-based methods [7], [8], feedback-linearization-based methods [9], [10], back-stepping and sliding-mode control [11], model-predictive control [12], [13], and nonlinear feedback control methods on the special Euclidean group [14], [15]. A review of some of the existing quadrotor control approaches can be found in [16]. Despite its success, the aforementioned planning-tracking paradigm lacks formal guarantees in the following sense: if the quadrotor is slightly deviating from the desired planned trajectory initially, it is not guaranteed that the employed controller will ensure tracking the desired path without colliding with obstacles.

Guaranteeing safety during reach-avoid control scenarios is generally challenging. One approach that provides formal guarantees is abstraction-based control synthesis [17]–[20], which is inapplicable to the high-dimensional quadrotor dynamics as abstraction-based computational requirements increase exponentially with the system dimension. Another interesting approach that can in theory provide safety guarantees relies on computing control contraction metrics [21], where robust invariant sets are estimated with incorporated feedback control, and outer bounds of the invariant sets are taken into account in the synthesis of nominal trajectories to be tracked [22]–[24]. Such estimates of the invariant sets are computationally demanding, and they rely on polynomial approximations of the quadrotor dynamics; hence, the formal guarantees are compromised. Besides the two aforementioned approaches, formal guarantees may be imposed by incorporating control barrier functions [25], which are obtained by solving optimization problems whose feasibility is not guaranteed in general. Up to our knowledge, incorporating control barrier functions for quadrotor systems has been successfully attained only for simple position and velocity bounds [26]. In summary, formally correct control approaches in the literature are limited when applied to quadrotor systems, which motivates the work presented herein.

To fulfill safety guarantees when synthesizing a quadrotor reach-avoid controller, we employ the standard planning-tracking paradigm, where we explicitly account for tracking errors when planning a desired trajectory. In principle, any tracking control method with theoretical stability guarantees can be utilized to derive uniform upper bounds of the tracking errors, and such bounds can then be used in designing trajectories with formal safety guarantees. Unfortunately, there exist several obstacles that prevent straightforward implementation of the tracking methods in the literature. For example, geometric tracking control [15], [27], [28], a variant of nonlinear feedback control on the special Euclidean group, was proposed with local exponential stability guarantees that are demonstrated using standard Lyapunov-type analysis. The analyses in [15], [27], [28] rely on conservative estimates which are convenient for proving stability but are impractical in planning applications. Besides, the theoretical analyses in some of the aforementioned works suffer from technical

Mohamed Serry, Haocheng Chang, and Jun Liu are with the Department of Applied Mathematics, University of Waterloo, Waterloo, Ontario, Canada (e-mail: {mserry, h48chang, j.liu}@uwaterloo.ca). The first two authors contributed equally to this manuscript. This work was funded in part by the Natural Sciences and Engineering Research Council of Canada and the Canada Research Chairs program.

issues associated with stability guarantees (see Remark 3), and that necessitates revisiting the stability analysis of geometric control. Moreover, the closed-loop quadrotor dynamics, when implementing geometric tracking control, possess a singularity whose analysis was overlooked. In [14], a nonlinear feedback tracking method was proposed, exhibiting impressive almost global asymptotic stability guarantees and addressing the potential singularity in the closed-loop quadrotor system. Unfortunately, the nature of the stability analysis in [14], which is mainly concerned with demonstrating asymptotic stability, makes it very challenging to derive closed-form error bounds that can be used in planning. Recently, an extension of the approach in [14] has been proposed in [13] utilizing model-predictive control to stabilize the translational tracking error, with similar almost global stability guarantees and, unfortunately, the same issue we highlighted for [14]. In this work, we aim to adapt the framework of geometric tracking control and revisit its stability analysis to derive closed-form tracking error bounds that can be used in trajectory planning, where we address the issues that we demonstrated above. Interestingly, revisiting the stability of geometric control reveals that the tracking error dynamics, when the geometric controller is implemented with *any* positive control gains, possess local exponential stability properties.

Our contribution in this paper is as follows.

- 1) We present a reach-avoid control synthesis framework for a quadrotor UAV with formal safety guarantees that adapts the standard planning-tracking paradigm, where nonlinear geometric control is employed for tracking and polynomial trajectory generation is based on Bézier curves. The proposed approach yields a desired (position) trajectory to be tracked and an initial set, where for any point in the initial set, the resulting quadrotor position follows the desired trajectory and reaches the target safely while avoiding obstacles, where velocity and thrust bounds are respected.
- 2) We revisit the stability analysis of the closed-loop quadrotor dynamics when geometric control is integrated. In our analysis, we show that under very mild assumptions (any positive choice for the control gains), the tracking error dynamics of the closed-loop system exhibit local exponential stability. Our analysis relies on using nonlinear differential inequalities to prove stability and tight estimates that result in accurate uniform bounds that can be used in the planning procedure. The set of initial values of the quadrotor system that guarantees safety is characterized by a set of nonlinear inequalities. We also introduce sufficient conditions to be imposed on the desired position trajectory for the well-definedness of the closed-loop quadrotor dynamics.
- 3) We present an efficient sampling-based planning algorithm that incorporates safe hyper-rectangular set-based computations to generate a safe tube that can be used in polynomial trajectory generation. The construction of the safe tube takes into account the uniform bounds of the tracking errors.
- 4) We propose a heuristic efficient approach that computes a safe polynomial trajectory, given as a piecewise-continuous Bézier curve, which lies within the generated safe tube, where uniform error bounds are taken into consideration in the synthesis procedure to ensure safety.

The organization of this paper is as follows: the necessary mathematical preliminaries are introduced in Section II; the quadrotor model equations are presented in Section III; The setup for the reach-avoid control synthesis problem is provided in Section IV; the geometric tracking control and the resulting error system are introduced in Section V; stability analysis of the error system is thoroughly investigated

in Section VI; the trajectory generation process is presented in detail in Section VII; the performance of our approach is displayed through numerical simulations in Section VIII; and the study is concluded in Section IX. Proofs of some of the technical results presented in this work are included in the Appendix.

II. PRELIMINARIES

Let \mathbb{R} , \mathbb{R}_+ , \mathbb{Z} , and \mathbb{Z}_+ denote the sets of real numbers, non-negative real numbers, integers, and non-negative integers, respectively, and $\mathbb{N} = \mathbb{Z}_+ \setminus \{0\}$. Let $[a, b]$, $]a, b[$, $[a, b[$, and $]a, b]$ denote the closed, open and half-open intervals, respectively, with endpoints a and b , and $[a; b]$, $]a; b[$, $[a; b[$, and $]a; b]$ stand for their discrete counterparts, e.g., $[a; b] = [a, b] \cap \mathbb{Z}$, and $[1; 4] = \{1, 2, 3\}$.

In \mathbb{R}^n , the relations $<$, \leq , \geq , and $>$ are defined component-wise, e.g., $a < b$, where $a, b \in \mathbb{R}^n$, iff $a_i < b_i$ for all $i \in [1; n]$. For $x \in \mathbb{R}^n$, $|x| \in \mathbb{R}^n$ is defined as $(|x|)_i := |x_i|$, $i \in [1; n]$. The n -dimensional vectors with zero and unit entries are denoted by 0_n and 1_n , respectively. Given two vectors $x, y \in \mathbb{R}^n$, $x \cdot y$ denotes the standard inner product of x and y ($x \cdot y = \sum_{i=1}^n x_i y_i$). For 3-dimensional vectors x and y , $x \times y$ denotes the cross product of x and y , i.e.,

$$x \times y := \begin{pmatrix} x_2 y_3 - x_3 y_2 \\ x_3 y_1 - x_1 y_3 \\ x_1 y_2 - x_2 y_1 \end{pmatrix}.$$

The space of n -dimensional real vectors is equipped with the Euclidean norm $\|\cdot\|$ ($\|x\| = \sqrt{x \cdot x}$, $x \in \mathbb{R}^n$). In addition, we make use of the maximal norm $\|\cdot\|_\infty$ defined as $\|x\|_\infty = \max_{i \in [1; n]} |x_i|$, $x \in \mathbb{R}^n$.

The n -dimensional closed unit balls with respect to $\|\cdot\|$ and $\|\cdot\|_\infty$ are denoted by \mathbb{B}_n and \mathbb{B}_n^∞ , respectively (note that $\mathbb{B}_n \subseteq \mathbb{B}_n^\infty$). Given $M \subseteq \mathbb{R}^n$, $\text{int}(M)$ denotes the interior of M , i.e., $\text{int}(M) := \{m \in M \mid m + r\mathbb{B}_n \subseteq M \text{ for some } r > 0\}$. The convex hull of N points in \mathbb{R}^n , x_1, x_2, \dots, x_N , is denoted by $\text{conv}(x_1, x_2, \dots, x_N)$. Given $M, N \subseteq \mathbb{R}^n$, $M \setminus N$ (set difference of M and N) denotes the set $\{x \in M \mid x \notin N\}$, $M + N$ (Minkowski sum of M and N) denotes the set $\{y + z \mid y \in M, z \in N\}$, and $M - N$ (Minkowski or Pontryagin difference of M and N (see, e.g., [29])) denotes the set $\{z \in \mathbb{R}^n \mid z + N \subseteq M\}$. Given a finite set M , $\text{card}(M)$ denotes the cardinality (number of elements) of M . Given $f: X \rightarrow Y$ and $C \subseteq X$, $f(C) := \{f(c) \mid c \in C\}$.

For $a, b \in (\mathbb{R} \cup \{-\infty, \infty\})^n$, $a \leq b$, the hyper-rectangle $\llbracket a, b \rrbracket$ denotes the set $\{x \in \mathbb{R}^n \mid a \leq x \leq b\}$, where, assuming a and b are finite, $\text{center}(\llbracket a, b \rrbracket) := (a + b)/2$ and $\text{radius}(\llbracket a, b \rrbracket) := (b - a)/2$. Note that $\mathbb{B}_n^\infty = \llbracket -1_n, 1_n \rrbracket$.

The identity map (matrix) on \mathbb{R}^n is denoted by I_n and the $n \times m$ zero matrix is denoted by $0_{n \times m}$. The transpose of an $n \times m$ matrix A is denoted by A^\top . For a matrix-valued function $A: I \subseteq \mathbb{R} \rightarrow \mathbb{R}^{n \times m}$, we define $A^\top(t) := (A(t))^\top$, $t \in I$. The trace and the determinant of an $n \times n$ matrix A are denoted by $\text{tr}(A)$ and $\det(A)$, respectively. Let $d = [d_1 \cdots d_n]^\top \in \mathbb{R}^n$, then the diagonal matrix with diagonal entries d_1, \dots, d_n , is denoted by $\text{diag}(d)$.

Let \mathcal{S}^n denote the space of $n \times n$ real symmetric matrices, i.e., $\mathcal{S}^n := \{A \in \mathbb{R}^{n \times n} \mid A = A^\top\}$. Note that the eigenvalues of a real symmetric matrix are real. Given $A \in \mathcal{S}^n$, $\underline{\lambda}(A)$ and $\overline{\lambda}(A)$ denote the minimum and maximum eigenvalues of A , respectively. For $n \times m$ real matrices, $\|\cdot\|$ is the matrix norm induced by the Euclidean norm ($\|A\| = \sqrt{\lambda(A^\top A)}$, $A \in \mathbb{R}^{n \times m}$).

A. Positive definite matrices

Let \mathcal{S}_{++}^n denote the set of $n \times n$ real symmetric positive definite matrices $\{A \in \mathcal{S}^n \mid \underline{\lambda}(A) > 0\}$ (see, e.g., [30, Chapter 8] and [31,

Chapter 6]). Given $A \in \mathcal{S}_{++}^n$, $A^{\frac{1}{2}}$ denotes the unique real symmetric positive definite matrix K satisfying $A = K^2$ [30, p. 220], and we define $A^{-\frac{1}{2}} := (A^{\frac{1}{2}})^{-1}$ (this is also equal to $(A^{-1})^{\frac{1}{2}}$ [30, p. 221]). Note that for $A \in \mathcal{S}_{++}^n$, $x^T A x = \|A^{\frac{1}{2}} x\|^2$ for all $x \in \mathbb{R}^n$. The following lemma states some useful estimates associated with positive definite matrices.

Lemma 1 (See the proof in the Appendix): Given $M, W \in \mathcal{S}_{++}^n$ and $x \in \mathbb{R}^n$, and $A \in \mathbb{R}^{m \times n}$, we have

- (a) $\underline{\lambda}(M)\|x\|^2 \leq x^T M x \leq \bar{\lambda}(M)\|x\|^2$,
- (b) $\underline{\lambda}(M^{-\frac{1}{2}} W M^{-\frac{1}{2}})\|M^{\frac{1}{2}} x\|^2 \leq \|W^{\frac{1}{2}} x\|^2$,
- (c) $\|A x\| \leq \|A M^{-\frac{1}{2}}\| \|M^{\frac{1}{2}} x\|$.

B. Special orthogonal and skew-symmetric matrices

Let $\text{SO}(3)$ denote the Lie group of real 3×3 proper orthogonal matrices and $\mathfrak{so}(3)$ denote the Lie algebra of real 3×3 skew-symmetric matrices, i.e., $\text{SO}(3) := \{A \in \mathbb{R}^{3 \times 3} | A^T = A^{-1}, \det(A) = 1\}$ and $\mathfrak{so}(3) := \{A \in \mathbb{R}^{3 \times 3} | A^T = -A\}$. The *hat map* $\wedge: \mathbb{R}^3 \rightarrow \mathfrak{so}(3)$ is defined as

$$\hat{x} := \begin{pmatrix} 0 & -x_3 & x_2 \\ x_3 & 0 & -x_1 \\ -x_2 & x_1 & 0 \end{pmatrix}, \quad x \in \mathbb{R}^3,$$

and the *vee map* $\vee: \mathfrak{so}(3) \rightarrow \mathbb{R}^3$ is the inverse of \wedge . Given a vector-valued function $x: I \subseteq \mathbb{R} \rightarrow \mathbb{R}^3$, we define $\hat{x}(t) := \widehat{x(t)}$, $t \in I$. The following lemma demonstrates some properties of the hat and vee maps, which can be easily verified by definition.

Lemma 2: For any $x, y \in \mathbb{R}^3$, $A \in \mathbb{R}^{3 \times 3}$ and $R \in \text{SO}(3)$, we have

$$\hat{x}^T = -\hat{x}, \quad (1)$$

$$\hat{x}y = x \times y = -y \times x = -\hat{y}x, \quad (2)$$

$$\text{tr}[A\hat{x}] = \frac{1}{2} \text{tr}[\hat{x}(A - A^T)] = -x^T(A - A^T)^{\vee}, \quad (3)$$

$$\hat{x}A + A^T \hat{x} = ((\text{tr}[A]I - A)x)^{\wedge}, \quad (4)$$

$$R\hat{x}R^T = \widehat{Rx}. \quad (5)$$

As $\text{SO}(3)$ is compact and connected, the exponential map, $A \mapsto \exp(A)$, from $\mathfrak{so}(3)$ to $\text{SO}(3)$ is surjective [32]. In addition, the hat map and its inverse establish a homeomorphism between \mathbb{R}^3 and $\mathfrak{so}(3)$. This consequently leads to the Euler-Rodrigues formula (see, e.g., [33], [34]):

Lemma 3: For each $R \in \text{SO}(3)$, there exists $x \in \mathbb{R}^3$ such that

$$R = \exp(\hat{x}) = \begin{cases} I_3 + \frac{\sin(\|x\|)}{\|x\|} \hat{x} + \frac{1 - \cos(\|x\|)}{\|x\|^2} \hat{x}^2, & x \neq 0_3, \\ I_3, & x = 0_3. \end{cases}$$

C. Differential inequalities

In our analysis of tracking error stability, we will resort to the following technical results concerning linear and nonlinear differential inequalities. The result below is the well-established Grönwall's lemma (see, e.g., [35, Lemma 1.1, p. 2]).

Lemma 4: Let $I \subseteq \mathbb{R}$ be an interval with a left endpoint t_0 , $b: I \rightarrow \mathbb{R}$ be continuous and $u: I \rightarrow \mathbb{R}$ be differentiable, satisfying $\dot{u}(t) \leq b(t)u(t)$, $t \in I$. Then, $u(t) \leq u(t_0)e^{\int_{t_0}^t b(s)ds}$, $t \in I$.

The following lemma is a modified version of [35, Lemma 4.1, p. 38], which is concerned with a Bernoulli-type nonlinear differential inequality that we will utilize in this work.

Lemma 5: Let $I \subseteq \mathbb{R}$ be an interval with a left endpoint t_0 , $b: I \rightarrow \mathbb{R}$ be continuous, $k: I \rightarrow \mathbb{R}$ be continuous and non-negative, and $u: I \rightarrow \mathbb{R}$ be positive and differentiable, satisfying $\dot{u}(t) \leq b(t)u(t) + k(t)\sqrt{u(t)}$, $t \in I$. Then, for all $t \in I$,

$$\sqrt{u(t)} \leq e^{\frac{1}{2} \int_{t_0}^t b(s)ds} \left(\sqrt{u(t_0)} + \frac{1}{2} \int_{t_0}^t k(s)e^{-\frac{1}{2} \int_{t_0}^s b(z)dz} ds \right).$$

As a consequence of the above lemma, we have the following result.

Lemma 6 (See the proof in the Appendix): Let $I \subseteq \mathbb{R}_+$ be an interval with 0 as the left endpoint, a_0, a_1, a_2, c be positive constants, and $u: I \rightarrow \mathbb{R}$ be a positive differentiable function, satisfying

$$\dot{u}(t) \leq -(a_0 - a_1 e^{-ct})u(t) + a_2 e^{-ct} \sqrt{u(t)}, \quad t \in I.$$

Then, for all $t \in I$,

$$\sqrt{u(t)} \leq e^{\frac{a_1}{2c}} \left(\sqrt{u(0)} e^{-\frac{a_0}{2}t} + \frac{a_2}{2} e^{-\frac{a_0}{2}t} \int_0^t e^{(\frac{a_0}{2}-c)s} ds \right).$$

D. Bézier curves

An n -dimensional Bézier curve (see, e.g., [36], [37]) $\mathfrak{B}: [0, T] \rightarrow \mathbb{R}^n$, of one segment, with $N + 1$ control points, is given by

$$\mathfrak{B}(t) = \sum_{i=0}^N c^i \mathfrak{b}_{i,N} \left(\frac{t}{T} \right), \quad t \in [0, T],$$

where $c^i \in \mathbb{R}^n$, $i \in [0; N]$, are the control points determining the shape of the curve, and $\mathfrak{b}_{i,N}: [0, 1] \rightarrow \mathbb{R}$, $i \in [0; N]$, are the Bernstein polynomials, which are defined by

$$\mathfrak{b}_{i,N}(\bar{t}) := \frac{i!}{(N-i)!} \bar{t}^i (1-\bar{t})^{N-i}, \quad \bar{t} \in [0, 1], \quad i \in [0; N],$$

where we use the convention that $0^0 := 1$. The initial and final values of \mathfrak{B} coincide with the first and last control points, respectively, i.e., $\mathfrak{B}(0) = c^0$, $\mathfrak{B}(T) = c^N$. Using the binomial theorem, it is easily verified that the Bernstein polynomials satisfy $\sum_{i=0}^N \mathfrak{b}_{i,N}(\bar{t}) = 1$, $\bar{t} \in [0, 1]$. This induces the useful property $\mathfrak{B}(t) \in \text{conv}(c^0, \dots, c^N)$, $t \in [0, T]$. Hence, the range of values of \mathfrak{B} can be controlled by tuning the control points c^0, \dots, c^N . In addition, the derivatives of Bézier curves are also Bézier curves. For example, $\dot{\mathfrak{B}}(t) = \sum_{i=0}^{N-1} \frac{N}{T} (c^{i+1} - c^i) \mathfrak{b}_{i,N-1}(\frac{t}{T})$, $\ddot{\mathfrak{B}}(t) = \sum_{i=0}^{N-2} \frac{N(N-1)}{T^2} (c^{i+2} - 2c^{i+1} + c^i) \mathfrak{b}_{i,N-2}(\frac{t}{T})$, $\dddot{\mathfrak{B}}(t) = \sum_{i=0}^{N-3} \frac{N(N-1)(N-2)}{T^3} (c^{i+3} - 3c^{i+2} + 3c^{i+1} - c^i) \mathfrak{b}_{i,N-3}(\frac{t}{T})$, and $\mathfrak{B}^{(4)}(t) = \sum_{i=0}^{N-4} \frac{N(N-1)(N-2)(N-3)}{T^4} (c^{i+4} - 4c^{i+3} + 6c^{i+2} - 4c^{i+1} + c^i) \mathfrak{b}_{i,N-4}(\frac{t}{T})$, $t \in [0, T]$. Therefore, the range of values of the derivatives of \mathfrak{B} can also be controlled by tuning the control points c^0, \dots, c^N .

III. QUADROTOR MODEL

Let $\{e_1, e_2, e_3\}$ be the standard basis of \mathbb{R}^3 (i.e., $= [e_1, e_2, e_3] = I_3$), which corresponds to the inertial reference (world) frame, where e_3 is pointing upward. Let $I \subset \mathbb{R}_+$ be an interval with 0 as the left endpoint, and let $t \in I$. The moving fixed-body frame of the quadrotor system is given by the time-varying orthonormal basis $\{b_1(t), b_2(t), b_3(t)\}$. The rotation matrix (attitude) that transforms the fixed-body frame into the inertial frame is $R(t) \in \text{SO}(3)$, where $b_i(t) = R(t)e_i$, $i \in [1; 3]$. The mass of the quadrotor is m and its inertia matrix, with respect to the moving fixed-body frame, is $J \in \mathbb{R}^{3 \times 3}$ (in fact, $J \in \mathcal{S}_{++}^3$). The quadrotor system consists of four identical rotors and propellers, with each pair capable of generating thrust and torque independently. The total thrust generated by the propellers is $f(t) \in \mathbb{R}$, and the total generated torque is $\tau(t) \in \mathbb{R}^3$. The position of the quadrotor's center of mass is $p(t) \in \mathbb{R}^3$, its velocity is $v(t) \in \mathbb{R}^3$, and the quadrotor's angular velocity, with respect to the fixed-body frame, is $\omega(t) \in \mathbb{R}^3$. Let $g \in \mathbb{R}_+$ denote the gravitational acceleration. Assuming negligible aerodynamic drag

forces¹, the governing equations of quadrotor dynamics are

$$\dot{p}(t) = v(t), \quad (6)$$

$$\dot{v}(t) = -ge_3 + m^{-1}f(t)R(t)e_3, \quad (7)$$

$$\dot{R}(t) = R(t)\hat{\omega}(t), \quad (8)$$

$$\dot{\omega}(t) = J^{-1}(-\omega(t) \times J\omega(t) + \tau(t)), \quad t \in I. \quad (9)$$

IV. PROBLEM FORMULATION

Let $\mathcal{X}_o = [\underline{x}_o, \bar{x}_o] \subseteq \mathbb{R}^3$ be a bounded hyper-rectangular operating domain and $\mathcal{X}_u = \bigcup_{i=1}^{N_u} [\underline{x}_u^{(i)}, \bar{x}_u^{(i)}] \subseteq \mathbb{R}^3$ be an unsafe set defined as a union of N_u hyper-rectangles. It is required that the quadrotor's position is always inside the operating domain, while avoiding the unsafe set. Let $\mathcal{X}_t = [\underline{x}_t, \bar{x}_t] \subseteq \mathbb{R}^3$ be a hyper-rectangular target set that we aim to drive the quadrotor's position into, where we assume $\mathcal{X}_t \subseteq \mathcal{X}_o \setminus \mathcal{X}_u$ ². Given a velocity bound $v_{\max} \in \mathbb{R}_+^3$, a thrust bound $f_{\max} \in \mathbb{R}_+$, a nominal initial point $(p_0, v_0, R_0, \omega_0) \in \mathbb{R}^3 \times \mathbb{R}^3 \times \text{SO}(3) \times \mathbb{R}^3$, where it is assumed that $p_0 \in \text{int}(\mathcal{X}_o) \setminus \mathcal{X}_u$, $|v_0| < v_{\max}$, and $(R_0, \omega_0) = (I_3, 0_3)$, find force and torque control laws such that there exists a finite time $T > 0$ and a non-singleton set containing $(p_0, v_0, R_0, \omega_0)$ in its relative interior, where for any initial value of the quadrotor system $(p(0), v(0), R(0), \omega(0))$ in that set, the corresponding trajectory of the quadrotor system and associated thrust satisfy

$$\begin{aligned} p(t) &\in \mathcal{X}_o \setminus \mathcal{X}_u, \\ |v(t)| &\leq v_{\max}, \\ |f(t)| &\leq f_{\max}, \quad t \in [0, T], \\ p(T) &\in \mathcal{X}_t. \end{aligned} \quad (10)$$

Remark 1: While we have stated previously that geometric tracking control will be employed in the reach-avoid control synthesis, the characterization of the thrust and torque control laws is still incomplete as we need to determine the desired (position) trajectory. In this work, we will introduce several conditions to be imposed on the desired trajectory to ensure formal safety as formulated in (10).

Remark 2: The framework presented herein can be applied to solve the safe set-stabilization problem $p(t) \in \mathcal{X}_o \setminus \mathcal{X}_u \forall t \geq 0$, and $\lim_{t \rightarrow \infty} \inf_{x \in \mathcal{X}_t} \|p(t) - x\| = 0$. In general, our approach can be employed when considering tracking control on an infinite time horizon, e.g., when addressing linear temporal logic [38] specifications.

To address the problem under consideration, our proposed approach relies on designing a desired trajectory with accompanying tracking controller, where the designed trajectory integrates uniform bounds that overestimate the tracking errors. We first introduce the tracking controller and rigorously analyze its stability properties, where we adapt the geometric control framework presented in [15].

V. GEOMETRIC CONTROL AND ERROR DYNAMICS

Let $I \subseteq \mathbb{R}_+$ be an interval with 0 as the left endpoint, and let $t \in I$. For tracking a desired trajectory, with desired position $p_d(t) \in \mathbb{R}^3$, rotation matrix $R_d(t) \in \text{SO}(3)$, and angular velocity $\omega_d(t) \in \mathbb{R}^3$,

¹Control of quadrotors with considerable drag forces has been analyzed in previous works (see, e.g., [13], [14]). The framework presented herein can be adapted to account for drag forces, where the thrust and torque control laws given in (16)–(18) are adjusted to account for such forces.

²The operating domain and the unsafe and target sets should account for the dimensions of the quadrotor to ensure collision avoidance and fully containing the quadrotor within the target region.

the tracking errors between the current and desired states are defined as follows [15]:

$$e_p(t) := p(t) - p_d(t), \quad (11)$$

$$e_v(t) := v(t) - \dot{p}_d(t), \quad (12)$$

$$e_R(t) := \frac{1}{2}(R_d^\top(t)R(t) - R^\top(t)R_d(t))^\vee, \quad (13)$$

$$e_\omega(t) := \omega - R^\top(t)R_d(t)\omega_d(t), \quad (14)$$

where e_p, e_v, e_R, e_ω are the error functions of the position, velocity, attitude, and angular velocity, respectively. We also present the configuration error function [15], [39]

$$\Psi(t) = \frac{1}{2}\text{tr}(I_3 - R_d^\top(t)R(t)), \quad t \in I. \quad (15)$$

We adopt the geometric control laws for the force and torque

$$f(t) = F_d(t) \cdot R(t)e_3, \quad (16)$$

$$F_d(t) = -k_p e_p(t) - k_v e_v(t) + mge_3 + m\ddot{p}_d(t), \quad (17)$$

$$\begin{aligned} \tau(t) &= -k_R e_R(t) - k_\omega e_\omega(t) + \omega(t) \times J\omega(t) \\ &\quad - J(\dot{\omega}(t)R^\top(t)R_d(t)\omega_d(t) - R^\top(t)R_d(t)\dot{\omega}_d(t)), \end{aligned} \quad (18)$$

$t \in I$, where k_p, k_v, k_R , and k_ω are positive control gains. As our problem is concerned with maneuvering within an operating domain to reach a target set while avoiding obstacles, the desired attitude, and angular velocity should ensure tracking the desired position p_d successfully. As in [39], we set

$$R_d(t) = [b_{1,d}(t), b_{2,d}(t), b_{3,d}(t)], \quad (19)$$

$$\dot{\omega}_d(t) = R_d^\top(t)\dot{R}_d(t), \quad (20)$$

and we choose, as in [40],

$$\begin{aligned} b_{1,d}(t) &= \frac{1}{\|F_d(t)\|} \begin{pmatrix} F_{d,3}(t) + \frac{(F_{d,2}(t))^2}{\|F_d(t)\| + F_{d,3}(t)} \\ -\frac{F_{d,1}(t)F_{d,2}(t)}{\|F_d(t)\| + F_{d,3}(t)} \\ -F_{d,1}(t) \end{pmatrix}, \\ b_{2,d}(t) &= \frac{1}{\|F_d(t)\|} \begin{pmatrix} -\frac{F_{d,1}(t)F_{d,2}(t)}{\|F_d(t)\| + F_{d,3}(t)}, \\ F_{d,3}(t) + \frac{(F_{d,1}(t))^2}{\|F_d(t)\| + F_{d,3}(t)} \\ -F_{d,2}(t) \end{pmatrix}, \\ b_{3,d}(t) &= \frac{F_d(t)}{\|F_d(t)\|}, \quad t \in I. \end{aligned} \quad (21)$$

We fix the time interval $I \subseteq \mathbb{R}_+$, where we assume 0 is the left endpoint, and consider the closed-loop quadrotor system (6)–(9), with (11)–(14) and (16)–(21), over I throughout the discussion below. Unless otherwise specified, we assume the control gains are fixed. In addition, it is assumed that p_d is four-times continuously differentiable over I , where p_d and its first four derivatives are assumed to be uniformly bounded over I .

Note that in the definition of ω_d in (20), we differentiate R_d with respect to time, which necessarily requires differentiating F_d (see equations (19) and (21)), where the evolution equations of p and v , given by (6) and (7), respectively, are used. Note also that ω_d depends on \ddot{p}_d and that $\dot{\omega}_d$, which is used in the torque law (18), depends on \ddot{p}_d , hence the four-times continuous differentiability assumption imposed on p_d .

In view of (21), it is important to ensure that

$$F_{d,3}(t) \neq -\|F_d(t)\|, \quad \|F_d(t)\| \neq 0 \quad (22)$$

for all $t \in I$ in order to have the closed-loop dynamics well-defined. In Section VI-C, we will introduce additional conditions on p_d that ensure existence (i.e., the functions p, v, R , and ω , defined through

the closed-loop system (6)–(9), with (11)–(14) and (16)–(21), do in fact exist over I and well-definedness (condition (22) holding).

In the subsequent analysis, we assume the second derivative of p_d to satisfy

$$|ge_3 + \ddot{p}_d(t)| \leq a_{\max}, \quad (23)$$

for all $t \in I$ and some specified $a_{\max} \in \mathbb{R}_+^3$. This bound will be useful in our stability analysis and when verifying the fulfillment of the thrust bound.

VI. STABILITY ANALYSIS

In this section, we analyze the evolution of the error terms (11)–(14). The evolution equations for the error functions are as follows.

Proposition 1 (See the proof in the Appendix): Assume that the functions p , v , R , and ω , given by (6)–(9), with (11)–(14) and (16)–(21), exist over I and that condition (22) holds over I . For $t \in I$, the derivatives of the error functions e_p , e_v , Ψ , e_R , and e_ω are given by

$$\dot{e}_p(t) = e_v(t), \quad (24)$$

$$\dot{e}_v(t) = -\frac{1}{m}(k_p e_p(t) + k_v e_v(t) - \Delta_f(t)), \quad (25)$$

$$\dot{\Psi}(t) = e_R(t) \cdot e_\omega(t), \quad (26)$$

$$\dot{e}_R(t) = \mathcal{C}(t)e_\omega(t), \quad (27)$$

$$\dot{e}_\omega(t) = J^{-1}(-k_R e_R(t) - k_\omega e_\omega(t)), \quad (28)$$

where

$$\mathcal{C}(t) := \frac{1}{2}(\text{tr}[R^\top(t)R_d(t)]\mathbf{I}_3 - R^\top(t)R_d(t)), \quad (29)$$

and

$$\Delta_f(t) := \|F_d(t)\|((b_{3,d}(t) \cdot b_3(t))b_3(t) - b_{3,d}(t)). \quad (30)$$

The following technical results will be useful in proving the stability of the error evolution equations. For these results, we assume that the functions p , v , R , and ω , given by (6)–(9), with (11)–(14) and (16)–(21), exist over I and that condition (22) holds over I . The result below follows by a direct application of the triangle inequality.

Lemma 7: Assume (23) holds and let $t \in I$. Then,

$$\|F_d(t)\| \leq \|k_p e_p(t) + k_v e_v(t)\| + m\|a_{\max}\|.$$

Lemma 8 (See the proof in the Appendix): Let $t \in I$. Then, $\|\mathcal{C}(t)\| \leq 1$.

Lemma 9 (See the proof in the Appendix): Let $t \in I$. Then, $\|e_R(t)\|^2 = \Psi(t)(2 - \Psi(t))$, and

$$\frac{1}{2}\|e_R(t)\|^2 \leq \Psi(t).$$

In addition, if there exists a positive constant ψ such that $\Psi(t) \leq \psi < 2$. Then,

$$\Psi(t) \leq \frac{1}{2-\psi}\|e_R(t)\|^2.$$

Lemma 10 (See the proof in the Appendix): Let $t \in I$. Under the assumption that $\Psi(t) \leq \psi$, for some constant $\psi \in]0, 2[$, we have

$$\|(b_{3,d}(t) \cdot b_3(t))b_3(t) - b_{3,d}(t)\| \leq \sqrt{\frac{2}{2-\psi}}\|e_R(t)\|.$$

Now, we present the first main result of this work concerning the dynamics of the error system (24)–(28).

Theorem 11: Assume that the functions p , v , R , and ω , given by (6)–(9), with (11)–(14) and (16)–(21), exist over I and that condition (22) holds over I . Moreover, assume condition (23) holds over I . Let $\alpha_\psi \in]0, 1[$ and $\bar{\Psi} \in]0, 2[$ be specified parameters and assume the following conditions hold:

$$\Psi(0) \leq \alpha_\psi \bar{\Psi}, \quad (31)$$

$$\frac{1}{2}e_\omega^\top(0)J e_\omega(0) \leq k_R(1 - \alpha_\psi)\bar{\Psi}. \quad (32)$$

Define

$$M_1 := \frac{1}{2} \begin{pmatrix} k_p \mathbf{I}_3 & c_1 \mathbf{I}_3 \\ c_1 \mathbf{I}_3 & m \mathbf{I}_3 \end{pmatrix}, \quad (33)$$

$$W_1 := \begin{pmatrix} \frac{c_1 k_p}{m} \mathbf{I}_3 & \frac{c_1 k_v}{2m} \mathbf{I}_3 \\ \frac{c_1 k_v}{2m} \mathbf{I}_3 & (k_v - c_1) \mathbf{I}_3 \end{pmatrix}, \quad (34)$$

$$M_{2,1} := \frac{1}{2} \begin{pmatrix} k_R \mathbf{I}_3 & c_2 \mathbf{I}_3 \\ c_2 \mathbf{I}_3 & J \end{pmatrix}, \quad M_{2,2} := \frac{1}{2} \begin{pmatrix} \frac{2k_R}{2-\bar{\Psi}} \mathbf{I}_3 & c_2 \mathbf{I}_3 \\ c_2 \mathbf{I}_3 & J \end{pmatrix}, \quad (35)$$

$$W_2 := \begin{pmatrix} c_2 k_R J^{-1} & \frac{c_2 k_\omega}{2} J^{-1} \\ \frac{c_2 k_\omega}{2} J^{-1} & (k_\omega - c_2) \mathbf{I}_3 \end{pmatrix}, \quad (36)$$

where c_1 and c_2 are constants, satisfying

$$0 < c_1 < \min \left(\sqrt{k_p m}, \frac{4mk_p k_v}{k_v^2 + 4mk_p} \right), \quad (37)$$

$$0 < c_2 < \min \left(\sqrt{k_R \bar{\Delta}(J)}, \frac{4\bar{\Delta}(J)k_R k_\omega}{k_\omega^2 + 4\bar{\Delta}(J)k_R} \right). \quad (38)$$

Moreover, define

$$z_1(t) := \begin{pmatrix} e_p(t) \\ e_v(t) \end{pmatrix}, \quad z_2(t) := \begin{pmatrix} e_R(t) \\ e_\omega(t) \end{pmatrix}, \quad t \in I,$$

and

$$V_1(t) := z_1^\top(t)M_1 z_1(t), \quad (39)$$

$$V_2(t) := \frac{1}{2}e_\omega^\top(t)J e_\omega(t) + k_R \Psi(t) + c_2 e_R(t) \cdot e_\omega(t), \quad (40)$$

$$V(t) := V_1(t) + V_2(t), \quad t \in I. \quad (41)$$

Then, $M_1, W_1, M_{2,1}, M_{2,2}, W_2 \in \mathcal{S}_{++}^6$. Furthermore, for all $t \in I$,

$$z_2^\top(t)M_{2,1} z_2(t) \leq V_2(t) \leq z_2^\top(t)M_{2,2} z_2(t), \quad (42)$$

$$V_2(t) \leq V_2(0)e^{-2\beta t}, \quad (43)$$

$$\sqrt{V(t)} \leq \mathcal{L}(V_1(0), V_2(0), t), \quad (44)$$

where, for $x, y, t \in \mathbb{R}_+$,

$$\mathcal{L}(x, y, t) := \mathcal{L}_1(x, y, t) + \mathcal{L}_2(y, t), \quad (45)$$

$$\mathcal{L}_1(x, y, t) := e^{\frac{\alpha_1 \sqrt{y}}{2\beta}} \sqrt{x + y} e^{-\frac{\alpha_0}{2} t}, \quad (46)$$

$$\mathcal{L}_2(y, t) := e^{\frac{\alpha_1 \sqrt{y}}{2\beta}} \frac{\alpha_2 \sqrt{y}}{2} e^{-\frac{\alpha_0}{2} t} \int_0^t e^{(\frac{\alpha_0}{2} - \beta)s} ds, \quad (47)$$

and β , α_0 , α_1 , and α_2 , are given by equations (48), (49), (50), and (51), respectively.

Proof: The proof presented herein is based on the proof presented in the archived version of [15] with significant refinements and adaptations. The conditions on c_1 and c_2 , given by (37) and (38), respectively, ensure the positive definiteness of M_1 , W_1 , $M_{2,1}$, $M_{2,2}$, and W_2 and that can be verified through Schur complement [41, Theorem 1.12, p. 34].

Next, we analyze V_2 . Define $\tilde{V}_2: I \rightarrow \mathbb{R}_+$ as

$$\tilde{V}_2(t) = \frac{1}{2}e_\omega(t) \cdot J e_\omega(t) + k_R \Psi(t), \quad t \in I.$$

Then, considering (26) and (28), we have

$$\begin{aligned} \dot{\tilde{V}}_2(t) &= e_\omega(t) \cdot J \dot{e}_\omega(t) + k_R \dot{\Psi}(t) \\ &= e_\omega(t) \cdot (-k_R e_R(t) - k_\omega e_\omega(t)) + k_R e_R(t) \cdot e_\omega(t) \\ &= -k_\omega e_\omega(t) \cdot e_\omega(t) \leq 0, \quad t \in I. \end{aligned}$$

This shows that \tilde{V}_2 is a decreasing function of time, where $\tilde{V}_2(t) \leq \tilde{V}_2(0)$, $t \in I$. Then, by considering conditions (31) and (32), we get

$$\begin{aligned} \tilde{V}_2(0) &= \frac{1}{2}e_\omega(0) \cdot J e_\omega(0) + k_R \Psi(0) \\ &\leq k_R(1 - \alpha_\psi)\bar{\Psi} + k_R \alpha_\psi \bar{\Psi} = k_R \bar{\Psi}. \end{aligned}$$

$$\beta := \frac{\lambda(M_{2,2}^{-\frac{1}{2}}W_2M_{2,2}^{-\frac{1}{2}})}{2}, \quad (48)$$

$$\alpha_0 := \min\left(\lambda(M_1^{-\frac{1}{2}}W_1M_1^{-\frac{1}{2}}), 2\beta\right), \quad (49)$$

$$\alpha_1 := \left\| \left[\frac{c_1}{m} I_3, I_3 \right] M_1^{-\frac{1}{2}} \right\| \left\| [k_p I_3, k_v I_3] M_1^{-\frac{1}{2}} \right\| \left\| [I_3, 0_{3 \times 3}] M_{2,1}^{-\frac{1}{2}} \right\| \sqrt{\frac{2}{2-\Psi}}, \quad (50)$$

$$\alpha_2 := m \|a_{\max}\| \left\| \left[\frac{c_1}{m} I_3, I_3 \right] M_1^{-\frac{1}{2}} \right\| \left\| [I_3, 0_{3 \times 3}] M_{2,1}^{-\frac{1}{2}} \right\| \sqrt{\frac{2}{2-\Psi}}. \quad (51)$$

Therefore, and as $\Psi(\cdot)$ and $e_\omega^\top(\cdot)J e_\omega(\cdot)$ are nonnegative functions of time, $\Psi(t) \leq \tilde{V}_2(t)/k_R \leq \tilde{V}_2(0)/k_R \leq \bar{\Psi} < 2$ for all $t \in I$. So, with the assumptions on $e_\omega(0)$ and $\Psi(0)$ given in (32) and (31), respectively, we have, using Lemma 9,

$$\frac{1}{2} \|e_R(t)\|^2 \leq \Psi(t) \leq \frac{1}{2-\bar{\Psi}} \|e_R(t)\|^2, \quad t \in I,$$

and consequently, equation (42) follows.

Now, we illustrate the exponential decay of V_2 . Differentiating V_2 with respect to time, where we substitute equations (27), (28), and (26) in, yields

$$\begin{aligned} \dot{V}_2(t) &= e_\omega(t) \cdot (-k_R e_R(t) - k_\omega e_\omega(t)) + k_R e_R(t) \cdot e_\omega(t) \\ &\quad + c_2(\mathcal{C}(t)e_\omega(t)) \cdot e_\omega(t) \\ &\quad + c_2 e_R(t) \cdot J^{-1}(-k_R e_R(t) - k_\omega e_\omega(t)), \quad t \in I. \end{aligned}$$

Using Lemma 8 and recalling the definition of W_2 in (36), we have

$$\begin{aligned} \dot{V}_2(t) &\leq -e_R(t) \cdot (c_2 k_R J^{-1}) e_R(t) - (k_\omega - c_2) e_\omega(t) \cdot e_\omega(t) \\ &\quad - e_R(t) \cdot (c_2 k_\omega J^{-1}) e_\omega(t) = -z_2^\top(t) W_2 z_2(t), \quad t \in I. \end{aligned}$$

The above estimate can be rewritten as $\dot{V}_2(t) \leq -\|W_2^{\frac{1}{2}} z_2(t)\|^2$, $t \in I$, and relation (42) can be written as $\|M_{2,1}^{\frac{1}{2}} z_2(t)\|^2 \leq V_2(t) \leq \|M_{2,2}^{\frac{1}{2}} z_2(t)\|^2$, $t \in I$. Therefore, using Lemma 1(b), $\dot{V}_2(t) \leq -\lambda(M_{2,2}^{-\frac{1}{2}} W_2 M_{2,2}^{-\frac{1}{2}}) V_2(t)$, $t \in I$. Using Lemma 4 and recalling the definition of β in equation (48), we obtain (43). As a consequence of the bounds (42) and (43), and using Lemma 1(c), we have

$$\begin{aligned} \|e_R(t)\| &\leq \left\| [I_3, 0_{3,3}] M_{2,1}^{-\frac{1}{2}} \right\| \sqrt{V_2(t)} \\ &\leq \left\| [I_3, 0_{3,3}] M_{2,1}^{-\frac{1}{2}} \right\| \sqrt{V_2(0)} e^{-\beta t}, \quad t \in I. \end{aligned}$$

Now, we analyze V_1 . Note that V_1 is nonnegative as a consequence of the positive definiteness of M_1 . Next, we obtain a bound on the derivative of V_1 . Differentiating V_1 with respect to time, considering (24) and (25), yields

$$\begin{aligned} \dot{V}_1(t) &= -\frac{c_1 k_p}{m} \|e_p(t)\|^2 - (k_v - c_1) \|e_v(t)\|^2 \\ &\quad - \frac{c_1 k_v}{m} e_p \cdot e_v(t) + \Delta_f(t) \cdot \left(\frac{c_1}{m} e_p(t) + e_v(t) \right), \quad t \in I. \end{aligned}$$

By recalling the definition of W_1 in (34), using the triangular inequality, and bounding $\|\Delta_f(\cdot)\|$ utilizing Lemmas 7 and 10, we have

$$\begin{aligned} \dot{V}_1(t) &\leq -z_1^\top(t) W_1 z_1(t) + \left\| \frac{c_1}{m} e_p(t) + e_v(t) \right\| \times \\ &\quad \sqrt{\frac{2}{2-\bar{\Psi}}} (\|k_p e_p(t) + k_v e_v(t)\| + m \|a_{\max}\|) \|e_R(t)\|, \end{aligned}$$

$t \in I$. Using Lemma 1(c) and the definition of V_1 , we have

$$\left\| \frac{c_1}{m} e_p(t) + e_v(t) \right\| \leq \left\| \left[\frac{c_1}{m} I_3, I_3 \right] M_1^{-\frac{1}{2}} \right\| \sqrt{V_1(t)},$$

$$\|k_p e_p(t) + k_v e_v(t)\| \leq \left\| [k_p I_3, k_v I_3] M_1^{-\frac{1}{2}} \right\| \sqrt{V_1(t)}, \quad t \in I.$$

Moreover, using Lemma 1(b) and the definition of V_1 , we have

$$-z_1^\top(t) W_1 z_1(t) \leq -\lambda(M_1^{-\frac{1}{2}} W_1 M_1^{-\frac{1}{2}}) V_1(t), \quad t \in I.$$

Subsequently, and using the definitions of α_1 and α_2 in equations (50) and (51), respectively, and the bound on $\|e_R(\cdot)\|$ using $\sqrt{V_2(\cdot)}$, the derivative of V_1 can be estimated as

$$\begin{aligned} \dot{V}_1(t) &\leq -\lambda(M_1^{-\frac{1}{2}} W_1 M_1^{-\frac{1}{2}}) V_1(t) \\ &\quad + \alpha_1 V_1(t) \sqrt{V_2(t)} + \alpha_2 \sqrt{V_1(t)} \sqrt{V_2(t)}, \quad t \in I. \end{aligned}$$

Now we consider the dynamics of V . Note that the non-negativity of V_1 and V_2 implies the non-negativity of V . In addition, we note that, using the definition of α_0 in (49),

$$\begin{aligned} -\lambda(M_1^{-\frac{1}{2}} W_1 M_1^{-\frac{1}{2}}) V_1(t) - \lambda(M_{2,2}^{-\frac{1}{2}} W_2 M_{2,2}^{-\frac{1}{2}}) V_2(t) &\leq \\ -\alpha_0 (V_1(t) + V_2(t)) = -\alpha_0 V(t), \quad t \in I. \end{aligned}$$

Combining the estimates of \dot{V}_1 and \dot{V}_2 and using the fact that $V_1(\cdot) \leq V(\cdot)$, the derivative of V can be estimated as

$$\begin{aligned} \dot{V}(t) &\leq -\lambda(M_1^{-\frac{1}{2}} W_1 M_1^{-\frac{1}{2}}) V_1(t) - \lambda(M_{2,2}^{-\frac{1}{2}} W_2 M_{2,2}^{-\frac{1}{2}}) V_2(t) \\ &\quad + \alpha_1 V_1(t) \sqrt{V_2(t)} + \alpha_2 \sqrt{V_1(t)} \sqrt{V_2(t)} \\ &\leq -\alpha_0 V(t) + \alpha_1 V(t) \sqrt{V_2(t)} + \alpha_2 \sqrt{V(t)} \sqrt{V_2(t)}, \quad t \in I. \end{aligned}$$

Assume that for some $t_0 \in I$, $V(t_0) = 0$. This implies that $V_2(t_0) = 0$, and as $V_2(t)$ is non-negative satisfying the condition of Grönwall's lemma, Lemma 4 tells us that $V_2(t) = 0$ for all $t \in I \cap [t_0, \infty[$. This consequently indicates that $\dot{V}(t) \leq -\alpha_0 V(t)$, $t \in I \cap [t_0, \infty[$, and using the non-negativity of V and Lemma 4, we have $V(t) = 0$, $t \in I \cap [t_0, \infty[$. Therefore, we may assume without loss of generality that $V(t) > 0$ for all $t \in I$. Using the bound on $V_2(\cdot)$ in (43) and rearranging we get

$$\dot{V}(t) \leq -(\alpha_0 - \alpha_1 \sqrt{V_2(0)} e^{-\beta t}) V(t) + \alpha_2 \sqrt{V_2(0)} e^{-\beta t} \sqrt{V(t)},$$

$t \in I$. Using Lemma 6, the proof is complete. \blacksquare

A. Local exponential stability

Herein, we state an important implication of Theorem 11. Assume $I = \mathbb{R}_+$. Note that the bounding function \mathcal{L} given in (45) is continuous over \mathbb{R}_+^3 and monotonically increasing with respect to the first two arguments, where $\mathcal{L}(0, 0, t) = 0$ for all $t \in I$. Moreover, for fixed $x, y \in \mathbb{R}_+$, $\mathcal{L}(x, y, t) \rightarrow 0$ as $t \rightarrow \infty$. By bounding the function \mathcal{L} , we can show that the zero of the error system is locally exponentially stable. Let $x, y, t \in \mathbb{R}_+$. Knowing that $\alpha_0/2$, defined

by (49), is less than or equal to β given in (48), the function \mathcal{L}_2 in (47) can be bounded as follows:

$$\begin{aligned}\mathcal{L}_2(y, t) &= e^{\frac{\alpha_1\sqrt{y}}{2\beta}} \frac{\alpha_2\sqrt{y}}{2} e^{-\frac{\alpha_0}{2}t} \int_0^t e^{(\frac{\alpha_0}{2}-\beta)s} ds \\ &\leq e^{\frac{\alpha_1\sqrt{y}}{2\beta}} \frac{\alpha_2\sqrt{y}}{2} e^{-\frac{\alpha_0}{2}t} \int_0^t e^{\nu s} ds \\ &\leq e^{\frac{\alpha_1\sqrt{y}}{2\beta}} \frac{\alpha_2\sqrt{y}}{2\nu} e^{-(\frac{\alpha_0}{2}-\nu)t},\end{aligned}$$

where $\nu \in]0, \alpha_0/2[$. We can also bound \mathcal{L}_1 in (46) as follows:

$$\mathcal{L}_1(x, y, t) \leq e^{\frac{\alpha_1\sqrt{y}}{2\beta}} \sqrt{x+y} e^{-(\frac{\alpha_0}{2}-\nu)t}.$$

Consequently, we have

$$\mathcal{L}(x, y, t) \leq e^{\frac{\alpha_1\sqrt{y}}{2\beta}} \left(\sqrt{x+y} + \frac{\alpha_2\sqrt{y}}{2\nu} \right) e^{-(\frac{\alpha_0}{2}-\nu)t},$$

and, using Theorem 11,

$$\sqrt{V(t)} \leq \sqrt{V(0)} e^{\frac{\alpha_1\sqrt{V(0)}}{2\beta}} \left(1 + \frac{\alpha_2}{2\nu} \right) e^{-(\frac{\alpha_0}{2}-\nu)t}, \quad t \in I.$$

The above inequality is valid whenever $(e_p(0), e_v(0), e_R(0), e_\omega(0))$ satisfies (31), and (32), which implies, with the help of the definitions of V_1 , V_2 , and V given by (39)–(41), the positive definiteness of M_1 and $M_{2,1}$, property (42), and Lemma 1(a), the local exponential stability of the error system (24)–(28); see, e.g., [42, Chapter 5]. While a similar result was derived in previous works, e.g., [15], additional assumptions were imposed on the control gains and the parameters c_1 and c_2 . Our result herein is stronger in the sense that we have local exponential stability for any positive choice of the control gains k_p , k_v , k_R , and k_ω .

Remark 3: In an archived and detailed version of [15], proving the exponential decay of the function V was attempted by asserting that, under some technical assumptions, $\|e_v(\cdot)\|$ is time-bounded. That assertion is based on differentiating the function $\dot{V}_1(\cdot) = \frac{1}{2} m e_v(\cdot) \cdot e_v(\cdot)$, a version of V_1 with c_1 and k_p are set to be zero, and showing that \dot{V}_1 is negative when $\|e_v(\cdot)\|$ is sufficiently large. Unfortunately, the estimate used in demonstrating the negativity of \dot{V}_1 is incorrect as it was derived without considering the fact that \dot{e}_v should satisfy (25), where k_p is still present, and that compromises the correctness of the stability proof.

B. Uniform bounds

In this section, we derive, using Theorem 11, some uniform bounds that can then be used in the synthesis of p_d . Note that \mathcal{L} given in (45), when the first two arguments are fixed, attains a maximum at a finite t that can be computed analytically. We consequently have the following uniform bound.

Corollary 1: Assume that the functions p , v , R , and ω , given by (6)–(9), with (11)–(14) and (16)–(21), exist over I and that condition (22) holds over I . In addition, assume (23), (31), and (32) hold. Let the functions V_1 , V_2 , and V be defined as in (39)–(41), where conditions (37) and (38) hold. Define, for $x, y \in \mathbb{R}_+$,

$$\mathcal{L}_u(x, y) := \max_{t \in \mathbb{R}_+} \mathcal{L}(x, y, t) = \mathcal{L}(x, y, t_m(x, y)), \quad (52)$$

where t_m is given by (53). Then,

$$\sqrt{V(t)} \leq \mathcal{L}_u(V_1(0), V_2(0)), \quad t \in I.$$

The uniform bound derived above and Lemma 1(c) can be used to estimate the deviation of the position and velocity from their desired values as follows:

Corollary 2: Assume that the functions p , v , R , and ω , given by (6)–(9), with (11)–(14) and (16)–(21), exist over I and that condition (22) holds over I . In addition, assume (23), (31), and (32) hold. Let the functions V_1 , V_2 , and V be defined as in (39)–(41), where conditions (37) and (38) hold. Define, for $x, y \in \mathbb{R}_+$,

$$\mathcal{L}_p(x, y) := \|[I_3, 0_{3 \times 3}] M_1^{-\frac{1}{2}}\| \mathcal{L}_u(x, y), \quad (54)$$

$$\mathcal{L}_v(x, y) := \|[0_{3 \times 3}, I_3] M_1^{-\frac{1}{2}}\| \mathcal{L}_u(x, y), \quad (55)$$

$$\mathcal{L}_f(x, y) := \|[k_p I_3, k_v I_3] M_1^{-\frac{1}{2}}\| \mathcal{L}_u(x, y), \quad (56)$$

then, for all $t \in I$,³

$$\|e_p(t)\| \leq \mathcal{L}_p(V_1(0), V_2(0)),$$

$$\|e_v(t)\| \leq \mathcal{L}_v(V_1(0), V_2(0)),$$

$$\|k_p e_p(t) + k_v e_v(t)\| \leq \mathcal{L}_f(V_1(0), V_2(0)).$$

C. Well-definedness of the closed-loop quadrotor system over any arbitrary time interval.

In Theorem 11, we assume that (22) holds and that the closed-loop system is well-defined over I . In the theorem below, we will show that, when imposing appropriate constraints on p_d , condition (22) is satisfied and well-definedness is guaranteed.

Theorem 12: Let conditions (23), (31), and (32) hold. In addition, assume

$$m\ddot{p}_{d,3}(t) \geq \alpha_f - mg + \varepsilon, \quad t \in I, \quad (57)$$

for some $\alpha_f, \varepsilon > 0$. Let V_1 , V_2 , and V be defined as in (39)–(41), where conditions (37) and (38) hold. If $\mathcal{L}_f(V_1(0), V_2(0))$, computed according to (56), satisfies

$$\alpha_f \geq \mathcal{L}_f(V_1(0), V_2(0)), \quad (58)$$

then the closed-loop quadrotor system is well-defined over I in the sense that the functions p , v , R , and ω , given by (6)–(9), with (11)–(14) and (16)–(21), exist and are differentiable over I . Moreover, condition (22) holds over I and the conclusions of Theorem 11 follow.

Proof: Recall the definitions of R_d and ω_d given by (19), (20), (21), and (17). Both R_d and ω_d depend on F_d , and F_d depends on e_p and e_v . Note that R_d , ω_d , and $\dot{\omega}_d$ are differentiable with respect to F_d whenever F_d is not zero and $\|F_d(\cdot)\| + F_{d,3}(\cdot)$ is not zero.

It follows from condition (37) that V_1 given by (39) is nonnegative over its domain of definition with the associated matrix M_1 being positive definite. Therefore, using Lemma 1(c) and the definition of \mathcal{L}_f in (56),

$$\begin{aligned}\|k_p e_p(0) + k_v e_v(0)\| &\leq \|[k_p I_3, k_v I_3] M_1^{-\frac{1}{2}}\| \sqrt{V_1(0)} \\ &= \mathcal{L}_f(V_1(0), 0) \\ &\leq \mathcal{L}_f(V_1(0), V_2(0)) \leq \alpha_f.\end{aligned}$$

Consequently,

$$\begin{aligned}F_{d,3}(0) &= -k_p e_{p,3}(0) - k_v e_{v,3}(0) + mg + m\ddot{p}_{d,3}(0) \\ &\geq -\mathcal{L}_f(V_1(0), V_2(0)) + mg \\ &\quad + \mathcal{L}_f(V_1(0), V_2(0)) - mg + \varepsilon = \varepsilon > 0,\end{aligned}$$

implying $\|F_d(0)\|, \|F_d(0)\| + F_{d,3}(0) > 0$. This shows that the right-hand sides of (6)–(9), with (11)–(14) and (16)–(21), are continuously

³As \mathcal{L} , given in equation (45), is monotonically increasing with respect to its first two arguments, then it follows, using the definition of \mathcal{L}_u , given by equation (52), that \mathcal{L}_u is monotonically increasing with respect to its two arguments. Therefore, \mathcal{L}_p , \mathcal{L}_u , and \mathcal{L}_f , given by (54), (55), and (56), respectively, are also monotonically increasing with respect to their arguments.

$$t_m(x, y) := \begin{cases} \max \left(\frac{1}{\frac{\alpha_0}{2} - \beta} \ln \left(\frac{\frac{\alpha_2 \beta \sqrt{y}}{2\beta - \alpha_0}}{\frac{\alpha_0}{2} \sqrt{x+y} + \frac{\alpha_0 \alpha_2 \sqrt{y}}{2(2\beta - \alpha_0)}} \right), 0 \right), & \frac{\alpha_0}{2} \neq \beta, y > 0, \\ \max \left(\frac{2(\alpha_2 \sqrt{y} - \alpha_0 \sqrt{x+y})}{\alpha_0 \alpha_2 \sqrt{y}}, 0 \right), & \frac{\alpha_0}{2} = \beta, y > 0, \\ 0, & \text{otherwise.} \end{cases} \quad (53)$$

differentiable with respect to t , p , v , R , and ω over a local neighborhood of $(p(0), v(0), R(0), \omega(0))$. Existence-uniqueness results for ordinary differential equations⁴ (see, e.g., [43, Theorem 3.2.1, Proposition 3.2.2., p. 82]) then guarantee the existence of a non-singleton interval $\tilde{I} \subset I$ containing zero over which the functions p , v , R , and ω are well-defined and differentiable.

Let $\tilde{I}_1 \subset I$ be the maximal interval of existence over which p , v , R , and ω are well-defined and differentiable, and define

$$\tilde{I}_2 := \{t \in \tilde{I}_1 \mid F_{d,3}(t) \leq 0\}, \quad \tilde{t} := \begin{cases} \inf \tilde{I}_2, & \tilde{I} \neq \emptyset, \\ \infty, & \text{otherwise,} \end{cases}$$

and $\tilde{I} := \{t \in \tilde{I}_1 \mid 0 \leq t < \tilde{t}\}$. The continuity of e_p , e_v , and \dot{p}_d (and consequently the continuity of F_d) over \tilde{I}_1 and the fact that $F_{d,3}(0) > 0$ ensure that \tilde{t} is positive. In addition, the definition of \tilde{I} ensures that condition (22) holds over \tilde{I} . We can then use the conclusions of Theorem 11, including Corollary 2, over \tilde{I} . Using Corollary 2, we have

$$\begin{aligned} F_{d,3}(t) &= -k_p e_{p,3}(t) - k_v e_{v,3}(t) + mg + m\dot{p}_{d,3}(t) \\ &\geq -\mathcal{L}_f(V_1(t), V_2(0)) + mg \\ &\quad + \mathcal{L}_f(V_1(t), V_2(0)) - mg + \varepsilon = \varepsilon > 0 \end{aligned}$$

for all $t \in \tilde{I}$. This uniform lower bound on $F_{d,3}$ and the definition of \tilde{I} imply $\tilde{I} = \tilde{I}_1$ as the definition of \tilde{t} implies it is infinite. Corollary 2 indicates that e_p and e_v are uniformly bounded over \tilde{I} (we can use theorem 11 to also show that e_R and e_ω are uniformly bounded over \tilde{I}). Moreover, and by construction, \dot{p}_d and its first four derivatives are uniformly bounded. Therefore, using the uniform boundedness of e_p and e_v , we have p and v uniformly bounded over \tilde{I} . Furthermore, by definition, R is uniformly bounded ($\|R(\cdot)\| = 1$) over \tilde{I} . The function ω_d , which depends on R_d and its derivative (see (20)), is uniformly bounded. Verifying this fact can be outlined as follows. Recalling the definition of R_d in (19), and using the chain rule, we have $\dot{\omega}_d(\cdot) = R_d^T(\cdot)\dot{R}_d(\cdot) = R_d^T(\cdot)\nabla_{F_d} R_d(\cdot)$, where $\nabla_{F_d} R_d$ is the derivative of R_d with respect to F_d . By construction, $\|R_d^T(\cdot)\| = 1$. Moreover, as $\varepsilon \leq F_{d,3}(\cdot) \leq \mathcal{L}_f(V_1(0), V_2(0)) + m\|a_{\max}\|$, the components of $\nabla_{F_d} R_d$ are uniformly bounded. Furthermore, $\dot{F}_d(\cdot)$, which is computed according to (82), is uniformly bounded over \tilde{I} due to the uniform boundedness of e_p , e_v , \dot{p}_d , and Δ_f . It then follows that $\dot{\omega}_d$ is uniformly bounded. Using equation (14) and the uniform boundedness of e_ω , R , R_d , and ω_d , ω is uniformly bounded over \tilde{I} . As \tilde{I} is the maximal interval of existence within I and that $p(\tilde{I})$, $v(\tilde{I})$, $R(\tilde{I})$, and $\omega(\tilde{I})$ are bounded, it follows that (see, e.g., [44, Corollary 4.10, p. 111], [43, Theorem 4.1.2, p. 112], and [45, Theorem 1.4.1, p. 18]) $\tilde{I}_1 = I$ and that completes the proof. ■

In the next corollary, we derive uniform bounds that are independent of both time and the values of V_1 and V_2 , where we utilize the monotonicity of \mathcal{L}_u . Such bounds can then be used to synthesize

⁴While R and R_d are matrix-valued functions, they can be cast as vector-valued functions through vectorization. Then, system (6)–(9) with the thrust and torque laws (16) and (18) can be viewed as a non-autonomous differential equation on a Euclidean space, and standard results on finite-dimensional differential equations can be applied.

a robust safe trajectory and an associated neighborhood of initial values.

We note that if conditions (31) and (32) hold, it follows, where Lemma 9 is used, that

$$\begin{aligned} V_2(0) &= \frac{1}{2} e_\omega(0) \cdot J e_\omega(0) + k_R \Psi(0) + c_2 e_R(0) \cdot e_\omega(0) \\ &\leq k_R \bar{\Psi} + c_2 \|e_R(0)\| \|e_\omega(0)\| \\ &\leq k_R \bar{\Psi} + c_2 \sqrt{2\Psi(0)} \|J^{-1/2}\| \|J^{1/2} e_\omega(0)\| \leq \bar{V}_2, \end{aligned}$$

where

$$\bar{V}_2 := \left(k_R + 2c_2 \sqrt{\frac{k_R}{\lambda(J)} \alpha_\psi (1 - \alpha_\psi)} \right) \bar{\Psi}. \quad (59)$$

Corollary 3: Let $\alpha_\psi \in]0, 1[$, $\bar{\Psi} \in]0, 2[$, and $\bar{V}_1 \in]0, \infty[$ be given and \bar{V}_2 is computed according to (59). Assume there exists a finite time $T > 0$ and a four-times continuously differentiable $p_d: [0, T] \rightarrow \mathbb{R}^3$ satisfying (23), and $m\dot{p}_{d,3}(t) \geq \mathcal{L}_f(\bar{V}_1, \bar{V}_2) - mg + \varepsilon$, $t \in [0, T]$, for some $\varepsilon > 0$. Then, for any initial value $(p(0), v(0), R(0), \omega(0))$ satisfying

$$\begin{aligned} \Psi(0) &\leq \alpha_\psi \bar{\Psi}, \\ \frac{1}{2} e_\omega^T(0) J e_\omega(0) &\leq k_R (1 - \alpha_\psi) \bar{\Psi}, \\ V_1(0) &\leq \bar{V}_1, \end{aligned} \quad (60)$$

the functions p , v , R , and ω , given by (6)–(9), with (11)–(14) and (16)–(21), exist over $[0, T]$ and condition (22) holds over $[0, T]$. Moreover, for all $t \in [0, T]$,

$$\begin{aligned} \|e_p(t)\| &\leq \mathcal{L}_p(\bar{V}_1, \bar{V}_2), \\ \|e_v(t)\| &\leq \mathcal{L}_v(\bar{V}_1, \bar{V}_2), \\ \|k_p e_p(t) + k_v e_v(t)\| &\leq \mathcal{L}_f(\bar{V}_1, \bar{V}_2), \end{aligned}$$

where \mathcal{L}_p , \mathcal{L}_v , and \mathcal{L}_f are given by (54), (55), and (56), respectively. A direct consequence of the above corollary is the following result which is the base of our trajectory generation procedure.

Theorem 13: Let $\alpha_\psi \in]0, 1[$, $\bar{\Psi} \in]0, 2[$, and $\bar{V}_1 \in]0, \infty[$ be given and \bar{V}_2 is computed according to (59). Assume

$$m\|a_{\max}\| + \mathcal{L}_f(\bar{V}_1, \bar{V}_2) \leq f_{\max}, \quad (61)$$

and that there exists a finite time $T > 0$ and a four-times continuously differentiable $p_d: [0, T] \rightarrow \mathbb{R}^3$ satisfying (23), and

$$\begin{aligned} p_d(t) &\in (\mathcal{X}_s - \mathcal{L}_p(\bar{V}_1, \bar{V}_2)\mathbb{B}_3) \setminus (\mathcal{X}_u + \mathcal{L}_p(\bar{V}_1, \bar{V}_2)\mathbb{B}_3), \\ |\dot{p}_d(t)| &\leq v_{\max} - \mathcal{L}_v(\bar{V}_1, \bar{V}_2) \mathbf{1}_3, \\ m\dot{p}_{d,3}(t) &\geq \mathcal{L}_f(\bar{V}_1, \bar{V}_2) - mg + \varepsilon, \\ p_d(T) &\in \mathcal{X}_t - \mathcal{L}_p(\bar{V}_1, \bar{V}_2)\mathbb{B}_3, \end{aligned} \quad (62)$$

$t \in [0, T]$, for some $\varepsilon > 0$, and \mathcal{L}_p , \mathcal{L}_v , and \mathcal{L}_f are given by (54), (55), and (56), respectively. Then, for any initial value $(p(0), v(0), R(0), \omega(0))$ satisfying (60), the functions p , v , R , and ω , given by (6)–(9), with (11)–(14) and (16)–(21), exist over $[0, T]$ and condition (22) holds over $[0, T]$. Moreover, the resulting position p and thrust f satisfy (10).

It is essential to show that the nominal point $(p_0, v_0, R_0, \omega_0)$ satisfies (60). The result below imposes conditions on p_d to ensure that the nominal point satisfies (60).

Lemma 14 (See the proof in the Appendix): If

$$p_d(0) = p_0, \dot{p}_d(0) = v_0, \ddot{p}_d(0) = 0_3, \dddot{p}_d(0) = 0_3. \quad (63)$$

Then, for $(p(0), v(0), R(0), \omega(0)) = (p_0, v_0, R_0, \omega_0)$, $R(0) = R_d(0)$, and $\omega(0) = \omega_d(0)$.

Remark 4: In order to satisfy (63) while having the first three conditions of (62) holding at $t = 0$, we need the choices of $\alpha_\psi \in]0, 1[$, $\bar{\Psi} \in]0, 2[$, and $\bar{\mathcal{V}}_1 \in]0, \infty[$ to ensure that

$$\begin{aligned} p_0 &\in (\mathcal{X}_s - \mathcal{L}_p(\bar{\mathcal{V}}_1, \bar{\mathcal{V}}_2)\mathbb{B}_3) \setminus (\mathcal{X}_u + \mathcal{L}_p(\bar{\mathcal{V}}_1, \bar{\mathcal{V}}_2)\mathbb{B}_3), \\ |v_0| &\leq v_{\max} - \mathcal{L}_v(\bar{\mathcal{V}}_1, \bar{\mathcal{V}}_2)1_3, \\ 0 &\geq \mathcal{L}_f(\bar{\mathcal{V}}_1, \bar{\mathcal{V}}_2) - mg + \varepsilon. \end{aligned}$$

The result above indicates that if $(p(0), v(0), R(0), \omega(0)) = (p_0, v_0, R_0, \omega_0)$, where p_d satisfies (63), then we have $\Psi(0) = \|e_\omega(0)\| = V_1(0) = 0$. Using a continuity argument, we have:

Corollary 4: Let $\alpha_\psi \in]0, 1[$, $\bar{\Psi} \in]0, 2[$, and $\bar{\mathcal{V}}_1 \in]0, \infty[$ be given and $\bar{\mathcal{V}}_2$ is computed according to (59). Assume p_d satisfies (23), (62), and (63), then there exists a neighborhood of $(p_0, v_0, R_0, \omega_0)$, relative to $\mathbb{R}^3 \times \mathbb{R}^3 \times \text{SO}(3) \times \mathbb{R}^3$, such that for any initial value in that neighborhood, the conditions in (60) hold.

VII. TRAJECTORY GENERATION

Let $\alpha_\psi \in]0, 1[$, $\bar{\Psi} \in]0, 2[$, and $\bar{\mathcal{V}}_1 \in]0, \infty[$ be given, $\bar{\mathcal{V}}_2$ be computed according to (59), and $\mathcal{L}_p(\bar{\mathcal{V}}_1, \bar{\mathcal{V}}_2)$, $\mathcal{L}_v(\bar{\mathcal{V}}_1, \bar{\mathcal{V}}_2)$, and $\mathcal{L}_f(\bar{\mathcal{V}}_1, \bar{\mathcal{V}}_2)$ be computed according to (54), (55), and (56), respectively. In this section, we illustrate how a desired trajectory p_d is computed. Our method combines some of the well-established planning approaches [46], [47] with efficient hyper-rectangular computations [48]. Informally speaking, our approach relies on a computing a safe tube of connected hyper-rectangles that do not intersect with the unsafe set, then conducting an optimization procedure that results in a polynomial trajectory that passes through the safe tube. Below, we illustrate how the safe tube is obtained.

A. Computing a safe tube

In view of Theorem 13, define

$$\begin{aligned} \tilde{\mathcal{X}}_o &:= \mathcal{X}_o - \mathcal{L}_p(\bar{\mathcal{V}}_1, \bar{\mathcal{V}}_2)\mathbb{B}_3^\infty, \\ \tilde{\mathcal{X}}_u^{(i)} &:= [\underline{x}_u^{(i)}, \bar{x}_u^{(i)}] + \mathcal{L}_p(\bar{\mathcal{V}}_1, \bar{\mathcal{V}}_2)\mathbb{B}_3^\infty, \quad i \in [1; N_u], \\ \tilde{\mathcal{X}}_u &:= \bigcup_{i=1}^{N_u} \tilde{\mathcal{X}}_u^{(i)}, \\ \tilde{\mathcal{X}}_t &:= \mathcal{X}_t - \mathcal{L}_p(\bar{\mathcal{V}}_1, \bar{\mathcal{V}}_2)\mathbb{B}_3^\infty. \end{aligned}$$

The sets above correspond to an inflated version of the unsafe set ($\tilde{\mathcal{X}}_u$) and deflated versions of the operating domain and target set ($\tilde{\mathcal{X}}_o$ and $\tilde{\mathcal{X}}_t$), where deflation and inflation are based on the position error bound $\mathcal{L}_p(\bar{\mathcal{V}}_1, \bar{\mathcal{V}}_2)$ defined by (54). Note that in our deflation and inflation procedure, we use the unit ball \mathbb{B}_3^∞ instead of \mathbb{B}_3 , which is more conservative yet computationally more efficient as Minkowski sums and differences of hyper-rectangles can be computed exactly by summing/subtracting centers and radii. The safe tube is obtained by generating $N_s + 1$ waypoints $p_0, p_1, \dots, p_{N_s} \in \mathbb{R}^3$, and associated vector radii $r_0, r_1, r_2, \dots, r_{N_s} \in \mathbb{R}_+^3$, satisfying

$$\begin{aligned} p_0 &= p_0, \\ p_{i+1} &\in p_i + [-r_i, r_i], \quad i \in [0; N_s - 1], \\ p_i + [-r_i, r_i] &\subseteq \tilde{\mathcal{X}}_o \setminus \tilde{\mathcal{X}}_u, \quad i \in [0; N_s - 1], \\ p_{N_s} + [-r_{N_s}, r_{N_s}] &\subseteq \tilde{\mathcal{X}}_t. \end{aligned} \quad (64)$$

Note that if a desired trajectory $p_d: [0, T] \rightarrow \mathbb{R}^3$ has values contained in the safe tube, with $p_d(T)$ contained in $p_{N_s} + [-r_{N_s}, r_{N_s}]$, the first and last conditions of (62) hold.

The waypoints and the associated safe radii can be estimated by integrating sampling-based approaches [47], with safe and efficient hyper-rectangular set-based computations [48]. The following technical lemmas illustrate how safe hyper-rectangular sets within the operating domain can be computed.

Lemma 15 (See the proof in the Appendix): Let $v \in \llbracket a, b \rrbracket \subseteq \mathbb{R}^n$, where $a, b \in \mathbb{R}^n$, $a \leq b$, then $\mathcal{H}(v, \llbracket a, b \rrbracket) \subseteq \llbracket a, b \rrbracket$, where

$$\mathcal{H}(v, \llbracket a, b \rrbracket) := v + \llbracket -r, r \rrbracket,$$

and $r = \text{radius}(\llbracket a, b \rrbracket) - |\text{center}(\llbracket a, b \rrbracket) - v|$.

Lemma 16 (See the proof in the Appendix): Let $x \in \mathbb{R}^n$ and $\llbracket a, b \rrbracket \subseteq \mathbb{R}^n$, where $a, b \in \mathbb{R}^n$, $a \leq b$. Moreover, let $r = \text{radius}(\llbracket a, b \rrbracket)$ and $c = \text{center}(\llbracket a, b \rrbracket)$. Then, $\min_{y \in \llbracket a, b \rrbracket} \|x - y\|_\infty = \|x - y^*\|_\infty$, where $y^* = \text{ClosestPoint}(x, \llbracket a, b \rrbracket)$,

$$(\text{ClosestPoint}(x, \llbracket a, b \rrbracket))_i := \begin{cases} x_i, & x_i \in [a_i, b_i], \\ c_i + r_i \text{sgn}(x_i - c_i), & \text{otherwise,} \end{cases}$$

$i \in [1; n]$, and $\text{sgn}(\cdot)$ is the signum function. Now, assume $x \notin \llbracket a, b \rrbracket$, let $\tilde{i} \in [1; p]$ such that $|x_{\tilde{i}} - y_{\tilde{i}}^*| = \|x - y^*\|_\infty > 0$, and define

$$\mathcal{S}(x, \llbracket a, b \rrbracket, \alpha) := \{z \in \mathbb{R}^n \mid |z_{\tilde{i}} - x_{\tilde{i}}| \leq \alpha \|x - y^*\|_\infty\},$$

where $\alpha \in [0, 1[$. Then, $\mathcal{S}(x, \llbracket a, b \rrbracket, \alpha) \cap \llbracket a, b \rrbracket = \emptyset$.

From Lemmas 15 and 16, we deduce:

Corollary 5: Let $y \in \tilde{\mathcal{X}}_o \setminus \tilde{\mathcal{X}}_u$, fix $\alpha \in [0, 1[$, and define

$$\mathfrak{R}(y, \tilde{\mathcal{X}}_o, \tilde{\mathcal{X}}_u, \alpha) := \mathcal{H}(y, \tilde{\mathcal{X}}_o) \cap \left(\bigcap_{i=1}^{N_u} \mathcal{S}(y, \tilde{\mathcal{X}}_u^{(i)}, \alpha) \right).$$

Then, $\mathfrak{R}(y, \tilde{\mathcal{X}}_o, \tilde{\mathcal{X}}_u, \alpha) \subseteq \tilde{\mathcal{X}}_o \setminus \tilde{\mathcal{X}}_u$.

Using the safe hyper-rectangles in Lemma 15 and Corollary 5, we construct a rapidly exploring random tree (RRT) $\mathcal{T} = (\mathcal{V}, \mathcal{E})$, with a set of vertices \mathcal{V} and a set of edges \mathcal{E} , such that each vertex (except the first one) is contained in a safe hyper-rectangular neighbor of the parent vertex. The metric used in constructing the tree is as follows: the distance between a sample point x_s and a point x_v in the vertex set \mathcal{V} is the distance between the sample point and a safe hyper-rectangle containing x_v , computed according to Lemma 5. If x_v happens to be associated with the shortest distance (among all the vertices of the tree), the new point added to the tree is a point within the safe hyper-rectangle that corresponds to that shortest distance.

Let N_v be the maximum number of vertices, $C_{\text{sample}} \in]0, 1[$ be a parameter that determines the percentage of points to be sampled from $\tilde{\mathcal{X}}_o$ and $\tilde{\mathcal{X}}_t$, and sample be a sampling function such that $\text{sample}(S)$ randomly generates a point from the set S . The random tree is then computed according to Algorithm 1, where the parameter α used in constructing the safe hyper-rectangles is user-defined. Once the tree \mathcal{T} is constructed, and assuming there exists a point $x_t \in \mathcal{V}$ such that $x_t \in \tilde{\mathcal{X}}_t$, a shortest path algorithm can then be conducted over \mathcal{T} , connecting p_0 and x_t , and resulting in $N_s + 1$ points $p_0 = p_0, p_1, \dots, p_{N_s} = x_t$. After that, the vector radii for the safe hyper-rectangles can be computed as follows:

$$\begin{aligned} r_i &= \text{radius}(\mathfrak{R}(p_i, \tilde{\mathcal{X}}_o, \tilde{\mathcal{X}}_u, \alpha)), \quad i \in [0; N_s - 1], \\ r_{N_s} &= \text{radius}(\mathcal{H}(p_{N_s}, \tilde{\mathcal{X}}_t)). \end{aligned} \quad (65)$$

By construction, the points $p_0, p_1, \dots, p_{N_s} \in \mathbb{R}^3$, and associated vector radii $r_0, r_1, r_2, \dots, r_{N_s} \in \mathbb{R}_+^3$ satisfy (64).

B. Piecewise Bézier curve

Once the safe tube is obtained, we compute the desired trajectory using Bézier curves. We assume p_d to be a piecewise continuous function with N_s segments, where each segment consists of $N_p + 1$ points. The parameter N_p is user-defined. Let δ_i , $i \in [1; N_s]$, be the duration of each segment, and define $t_0 = 0$, $t_i = t_{i-1} + \delta_i$, $i \in$

Algorithm 1: Constructing an RRT

```

1  $i \leftarrow 1, x_i \leftarrow p_0, \mathcal{V} \leftarrow \{x_i\}, \mathcal{E} \leftarrow \emptyset$ 
2 while  $i \leq N_v$  do
3   if  $i \leq C_{\text{sample}} N_v$  then
4      $x_s \leftarrow \text{sample}(\tilde{\mathcal{X}}_s \setminus \tilde{\mathcal{X}}_u)$ 
5   else
6      $x_s \leftarrow \text{sample}(\tilde{\mathcal{X}}_t)$ 
7   end
8    $d \leftarrow \infty, j \leftarrow 1$ 
9   while  $j \leq \text{card}(\mathcal{V})$  do
10     $d' \leftarrow \|x_s - \text{ClosestPoint}(x_s, \mathfrak{R}(x_j, \tilde{\mathcal{X}}_o, \tilde{\mathcal{X}}_u, \alpha))\|_\infty$ 
11    if  $d' < d$  then
12       $d \leftarrow d', i_{\text{near}} \leftarrow j$ 
13    end
14     $j \leftarrow j + 1$ 
15  end
16   $i \leftarrow i + 1$ 
17   $x_i \leftarrow \text{ClosestPoint}(x_s, \mathfrak{R}(x_{i_{\text{near}}}, \tilde{\mathcal{X}}_o, \tilde{\mathcal{X}}_u, \alpha))$ 
18   $\mathcal{V} \leftarrow \mathcal{V} \cup \{x_i\}, \mathcal{E} \leftarrow \mathcal{E} \cup \{(x_{i_{\text{near}}}, x_i)\}$ 
19  if  $x_i \in \tilde{\mathcal{X}}_t$  then
20    break
21  end
22 end
Result:  $\mathcal{T} = (\mathcal{V}, \mathcal{E})$ 

```

$[1; N_s]$, $T = \sum_{i=1}^{N_s} \delta_i$. Then, $p_d: [0, T] \rightarrow \mathbb{R}^3$ has the form (see Section II-D)

$$p_d(t) = \begin{cases} \sum_{i=0}^{N_p} c_1^i \mathbf{b}_{i,n} \left(\frac{t-t_0}{\delta_1} \right), & t \in [t_0, t_1], \\ \sum_{i=0}^{N_p} c_2^i \mathbf{b}_{i,n} \left(\frac{t-t_1}{\delta_2} \right), & t \in [t_1, t_2], \\ \vdots \\ \sum_{i=0}^{N_p} c_{N_s}^i \mathbf{b}_{i,n} \left(\frac{t-t_{N_s-1}}{\delta_{N_s}} \right), & t \in [t_{N_s-1}, t_{N_s}]. \end{cases} \quad (66)$$

The control points c_i^j , $i \in [1; N_s]$, $j \in [0; N_p]$, are required to satisfy the following set of constraints, which are based on Theorem 13 and Lemma 14⁵:

- the initial value of p_d is p_0 :

$$c_1^0 = \mathbf{p}_0, \quad (67)$$

- the initial value of \dot{p}_d is v_0 :

$$\frac{N_p}{\delta_1} (c_1^1 - c_1^0) = v_0, \quad (68)$$

- the initial value of \ddot{p}_d is 0_3 :

$$c_1^2 - 2c_1^1 + c_1^0 = 0_3, \quad (69)$$

- the initial value of $\ddot{\ddot{p}}_d$ is 0_3 :

$$c_1^3 - 3c_1^2 + 3c_1^1 - c_1^0 = 0_3, \quad (70)$$

- safety of the generated trajectory in the sense that $p_d(t) \in \mathbf{p}_{i-1} + \llbracket -\mathbf{r}_{i-1}, \mathbf{r}_{i-1} \rrbracket$, $t \in [t_{i-1}, t_i]$, $i \in [1; N_s]$:

$$c_i^j \in \mathbf{p}_{i-1} + \llbracket -\mathbf{r}_{i-1}, \mathbf{r}_{i-1} \rrbracket \quad \forall j \in [0; N_p], \quad i \in [1; N_s], \quad (71)$$

- continuity of p_d at the junction points:

$$c_i^{N_p} = c_{i+1}^0 \quad \forall i \in [1; N_s - 1], \quad (72)$$

⁵Additional constraints can be imposed if necessary such as requiring $\dot{p}_d(T) = \dot{p}_d(T) = 0_3$.

- satisfying the velocity bound $|\dot{p}_d(t)| \leq v_{\max} - \mathcal{L}_v(\bar{\mathcal{V}}_1, \bar{\mathcal{V}}_2) \mathbf{1}_3$, $t \in [0, T]$:

$$\left| \frac{N_p}{\delta_i} (c_i^{j+1} - c_i^j) \right| \leq v_{\max} - \mathcal{L}_v(\bar{\mathcal{V}}_1, \bar{\mathcal{V}}_2) \mathbf{1}_3, \quad (73)$$

$$j \in [0; N_p - 1], \quad i \in [1; N_s],$$

- continuity of \dot{p}_d at the junction points:

$$\frac{1}{\delta_i} (c_i^{N_p} - c_i^{N_p-1}) = \frac{1}{\delta_{i+1}} (c_{i+1}^1 - c_{i+1}^0) \quad \forall i \in [1; N_s - 1], \quad (74)$$

- satisfying the bound $|ge_3 + \ddot{p}_d(t)| \leq a_{\max}$, $t \in [0, T]$:

$$\left| \frac{N_p(N_p-1)}{\delta_i^2} (c_i^j - 2c_i^{j+1} + c_i^{j+2}) + ge_3 \right| \leq a_{\max}, \quad j \in [0; N_p - 2], \quad i \in [1; N_s], \quad (75)$$

- satisfying the condition $m\ddot{\ddot{p}}_{d,3}(t) \geq \mathcal{L}_f(\bar{\mathcal{V}}_1, \bar{\mathcal{V}}_2) - mg + \varepsilon$, $t \in [0, T]$:

$$\frac{mN_p(N_p-1)}{\delta_i^2} (c_{i,3}^j - 2c_{i,3}^{j+1} + c_{i,3}^{j+2}) \geq \mathcal{L}_f(\bar{\mathcal{V}}_1, \bar{\mathcal{V}}_2) - mg + \varepsilon, \quad j \in [0; N_p - 2], \quad i \in [1; N_s], \quad (76)$$

- continuity of \ddot{p}_d at the junction points:

$$\frac{1}{\delta_i^2} (c_i^{N_p} - 2c_i^{N_p-1} + c_i^{N_p-2}) = \frac{1}{\delta_{i+1}^2} (c_{i+1}^2 - 2c_{i+1}^1 + c_{i+1}^0), \quad i \in [1; N_s - 1], \quad (77)$$

- continuity of $\ddot{\ddot{p}}_d$ at the junction points:

$$\frac{1}{\delta_i^3} (c_i^{N_p} - 3c_i^{N_p-1} + 3c_i^{N_p-2} - c_i^{N_p-3}) = \frac{1}{\delta_{i+1}^3} (c_{i+1}^3 - 3c_{i+1}^2 + 3c_{i+1}^1 - c_{i+1}^0), \quad i \in [0; N_s - 1], \quad (78)$$

- continuity of $\ddot{\ddot{\ddot{p}}}_d$ at the junction points:

$$\frac{1}{\delta_i^4} (c_i^{N_p} - 4c_i^{N_p-1} + 6c_i^{N_p-2} - 4c_i^{N_p-3} + c_i^{N_p-4}) = \frac{1}{\delta_{i+1}^4} (c_{i+1}^4 - 4c_{i+1}^3 + 6c_{i+1}^2 - 4c_{i+1}^1 + c_{i+1}^0), \quad i \in [0; N_s - 1], \quad (79)$$

- the value of p_d at final time is in $\mathbf{p}_{N_s} + \llbracket -\mathbf{r}_{N_s}, \mathbf{r}_{N_s} \rrbracket$:

$$\mathbf{p}_{N_s} - \mathbf{r}_{N_s} \leq c_{N_s}^{N_p} \leq \mathbf{p}_{N_s} + \mathbf{r}_{N_s}. \quad (80)$$

Note that if the time durations $\delta_1, \dots, \delta_{N_s}$ are specified, the constraints (67)–(80) above are linear with respect to the control points. In Algorithm 2, we present a heuristic approach to determine the desired trajectory p_d by means of iterative linear programming. The heuristic approach relies on initially guessing the time T and incrementally increasing it until the constraints become feasible, where each duration δ_i is assumed to be a fraction of T that depends on the ratio of the distance between the consecutive two waypoints \mathbf{p}_{i-1} and \mathbf{p}_i over the total length of the piecewise linear curve connecting all the waypoints. We assume the value of N_p is given and fixed during the synthesis procedure.⁶

If the procedure in Algorithm 2 is successful, we have the resulting trajectory satisfying (23), (62), and (63). Therefore, the reach-avoid problem in this work is solved successfully, where the safe initial set containing $(p_0, v_0, R_0, \omega_0)$ is characterized by (60).

⁶The trajectory resulting from Algorithm 2 may be sub-optimal (e.g., in terms of jerk or snap). If optimality criteria are important to impose on the desired trajectory, then nonlinear optimization methods may be adopted (see, e.g., [3], [6], [46]).

Algorithm 2: Computing the desired trajectory

- 1 Define $l_i = \|\mathbf{p}_i - \mathbf{p}_{i-1}\|$, $i \in [1; N_s]$, $L = \sum_{i=1}^{N_s} l_i$,
 $q_i = \frac{l_i}{L}$, $i \in [1; N_s]$.
 - 2 Let T_0 be a positive parameter specifying an initial guess for the full time horizon and $\alpha_t > 1$ be a scaling parameter.
 - 3 Define $\delta_i = q_i T_0$, $i \in [1; N_s]$.
 - 4 With the values of δ_i , $i \in [1; N_s]$, defined in step 3, solve a linear program involving the control points c_i^j , $j \in [0; N_p]$, $i \in [1; N_s]$, while considering the constraints (67)–(80).
 - 5 If the linear program in step 4 is feasible, the resulting control points in addition to the time durations δ_i , $i \in [1; N_s]$, can then be used to obtain the desired trajectory according to equation (66).
 - 6 If the linear program in step 4 is infeasible, redefine T_0 as $T_0 := \alpha_T T_0$, and repeat steps 3 and 4.
-

VIII. NUMERICAL SIMULATIONS

Numerical quadrotor simulations (using MATLAB) incorporating the proposed control synthesis approach are conducted to demonstrate its performance and effectiveness. For the purpose of consistency, all calculations and computations are done on a computer with an i7-12700 CPU. The hyper-rectangular plots presented in this section are obtained with the MATLAB command `plotcube` [49].

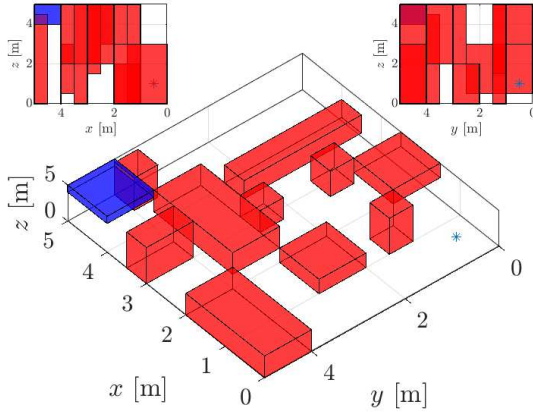


Fig. 1. The environment with ten obstacles as red boxes, one target set as the blue box, and the starting point as the blue asterisk. The top left corner is the view along the negative direction of the y-axis, and the top right corner is the view along the positive direction of the x-axis.

The parameters of the quadrotor are adopted from [15], where

$$J = \text{diag}([0.0820, 0.0845, 0.1377]^T) \text{ kg} \cdot \text{m}^2, \quad m = 4.34 \text{ kg}.$$

A. Reach-avoid problem setup

We consider a reach-avoid control scenario, where the operating domain is defined as a cube with edges measuring 5 meters each ($\mathcal{X}_o = \llbracket [0, 0, 0]^T, [5, 5, 5]^T \rrbracket$), the target set is given by $\mathcal{X}_t = \llbracket [4, 4, 4]^T, [5, 5, 5]^T \rrbracket$, and the unsafe set is given as a union of ten hyper-rectangles. The initial nominal position of the quadrotor is $p_0 = [0.5, 0.5, 1]^T$ and the initial nominal velocity is $v_0 = \mathbf{0}_3$. The operating domain, the target and the unsafe sets, and the initial nominal position are depicted in Figure 1. We let $v_{\max} = [2, 2, 2]^T$,

$f_{\max} = 2mg = 85.1508 \text{ N}$, and $a_{\max} = [1, 1, 10]^T$. The control synthesis process starts by setting $\bar{\Psi} = 0.005$, $\alpha_\psi = 0.4$, $\bar{V}_1 = 0.4$.

B. Gain tuning through optimization

While our theoretical results imply local exponential stability of the closed-loop quadrotor dynamics for any choice of positive control gains, that choice should ensure that the theoretical uniform bounds, which depend implicitly on the control gains, are not too conservative. In particular, we want the gains choice to result in small values for the uniform bounds $\mathcal{L}_p(\bar{V}_1, \bar{V}_2)$, $\mathcal{L}_v(\bar{V}_1, \bar{V}_2)$, and $\mathcal{L}_f(\bar{V}_1, \bar{V}_2)$, where \bar{V}_2 is computed according to (59). Let $\gamma_1, \gamma_2 \in]0, 1[$ be parameters that determine the values of c_1 and c_2 , used in the definitions of the functions V_1 and V_2 in (39) and (40), respectively, through the relations

$$c_1 = \gamma_1 \min \left(\sqrt{k_p m}, \frac{4mk_p k_v}{k_v^2 + 4mk_p} \right),$$

$$c_2 = \gamma_2 \min \left(\sqrt{k_R \Delta(J)}, \frac{4\Delta(J)k_R k_\omega}{k_\omega^2 + 4\Delta(J)k_R} \right).$$

The above relations and the bounds on γ_1 and γ_2 ensure that conditions (37) and (38) hold. Let $\underline{k}, \bar{k} \in \mathbb{R}_+ \setminus \{0\}$ be user-defined positive lower and upper bounds on the control gains, respectively, and w_1, w_2 , and w_3 be positive weights to be assigned to the uniform bounds during the optimization process. The control gains, and the parameters γ_1 and γ_2 are then determined by solving the following nonlinear optimization problem, where the uniform bounds $\mathcal{L}_p(\bar{V}_1, \bar{V}_2)$, $\mathcal{L}_v(\bar{V}_1, \bar{V}_2)$, and $\mathcal{L}_f(\bar{V}_1, \bar{V}_2)$ are functions of the gains through the relations (52), (54), (55), (56), and (43) and the arguments \bar{V}_1 and \bar{V}_2 are dropped:

$$\begin{aligned} \min_{k_p, k_v, k_R, k_\omega, \gamma_1, \gamma_2} \quad & w_1 \mathcal{L}_p + w_2 \mathcal{L}_v + w_3 \mathcal{L}_f, \\ \text{s.t.} \quad & \underline{k} \leq k_p, k_v, k_R, k_\omega \leq \bar{k}, \\ & 0 < \gamma_1, \gamma_2 < 1. \end{aligned} \quad (81)$$

We set the gain bounds to be $\underline{k} = 0.1$, $\bar{k} = 30$ and choose the weight values $w_1 = 15$, $w_2 = 1$, $w_3 = 1$. The gains are obtained by solving (81) with Simulated Annealing [50], a stochastic global search optimization algorithm. The MATLAB built-in function `simulannealbnd` is adopted. With the initial guess

$$k_p = 10, \quad k_v = 10, \quad k_R = 10, \quad k_\omega = 10, \quad \gamma_1 = 0.5, \quad \gamma_2 = 0.5,$$

the optimized control gains and coefficients are obtained as

$$k_p = 18.5058, \quad k_v = 5.6704, \quad k_R = 23.5537, \quad k_\omega = 1.4309,$$

$$\gamma_1 = 0.5500, \quad \gamma_2 = 0.6047.$$

The average computing time for obtaining the gains via optimization is 0.8934 seconds. The resulting value of \bar{V}_2 is 24.4053 and the resulting uniform bounds are $\mathcal{L}_p(\bar{V}_1, \bar{V}_2) = 0.3374 \text{ m}$, $\mathcal{L}_v(\bar{V}_1, \bar{V}_2) = 0.6968 \text{ m/s}$, and $\mathcal{L}_f(\bar{V}_1, \bar{V}_2) = 6.2445 \text{ N}$, with $\mathcal{L}_u(\bar{V}_1, \bar{V}_2) = 0.9737$. In addition, the theoretical bound on thrust is

$$\bar{\mathcal{F}} := \mathcal{L}_f(\bar{V}_1, \bar{V}_2) + m \|a_{\max}\| = 50.0763 \text{ N},$$

which is less than the specified thrust bound f_{\max} .

C. Safe tube and trajectory synthesis

Next, we construct a safe tube that consists of connected hyper-rectangles, through which the desired trajectory is synthesized. The safe tube is obtained by first constructing an RRT according to Algorithm 1, then obtaining a set of waypoints by conducting a shortest path algorithm over the RRT, and finally computing the

radii of the hyper-rectangles of the safe tube according to (65). The parameters in Algorithm 1 are chosen to be $\alpha = 0.9$, $N_v = 400$, $C_{\text{sampling}} = 0.9$. The resulting safe tube consists of fifteen hyper-rectangles depicted in Figure 2, where the associated computational time is 0.06 seconds.

Next, we construct the desired trajectory given as a piecewise Bézier curve with fifteen segments, where each segment is parameterized by fifteen control points ($N_p = 14$). We implement Algorithm 2 for the trajectory synthesis, where we set $\alpha_T = 1.1$, $T_0 = 10$, and we use $\varepsilon = 10^{-6}$ for the constraint given in equation (76). The resulting trajectory, with time duration $T = 45.94$ seconds, is depicted in Figure 3. The trajectory computation based on Algorithm 2 required 0.89 seconds of CPU time.

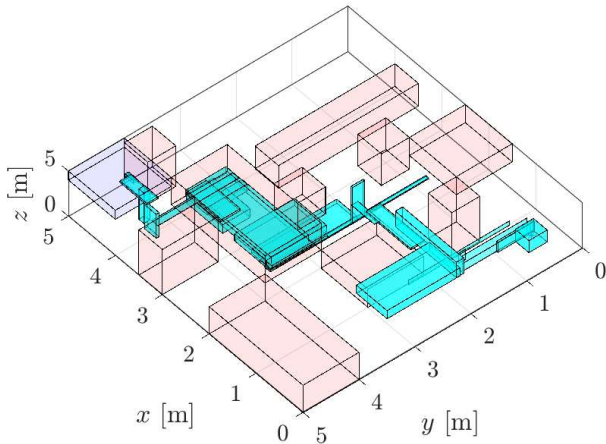


Fig. 2. The safe tube is the union of the cyan boxes. Note that the safe tube does not intersect with the unsafe set (union of the light red boxes), where the last box of the safe tube lies within the target set (blue box).

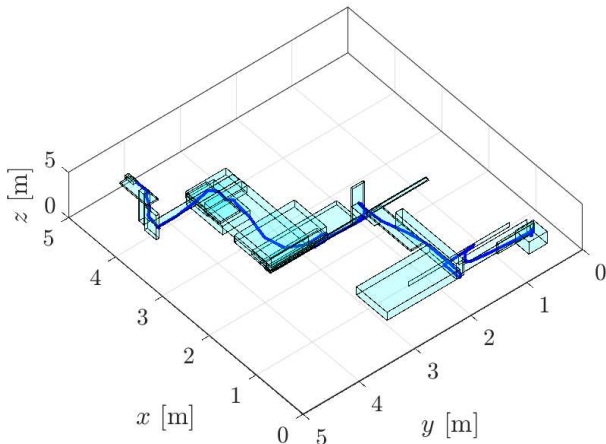


Fig. 3. The generated desired trajectory p_d is shown as the blue curve, which lies within the safe tube (union of cyan boxes).

D. Initial points generation

As demonstrated in Theorem 13, the safety of the closed-loop quadrotor system is guaranteed if the initial conditions satisfy (60). The safe initial set is characterized by (60) by means of sampling, where sample points satisfying (60) are considered safe, whereas

those violating (60) are deemed unsafe. We consider two distinct cases for sampling. In the first case, the initial position error is sampled through the relation $e_p(0) = \text{sample}(0.21[-1_3, 1_3])$, with the initial velocity error $e_v(0)$ attitude error $e_R(0)$, and angular velocity error $e_\omega(0)$ all set to zero. In the second case, the initial attitude error $e_R(0)$ is determined by (14) with $R(0) = e^{(\text{sample}(0.1[-1_3, 1_3]))^\wedge}$ (refer to Lemma 3), while $e_p(0) = e_v(0) = e_\omega(0) = 0$ (This results in $R_d(0) = I_3$). In each case, one million points are sampled, with safe points marked red and unsafe points marked blue, as illustrated in Figure 4. The cross-sectional figures shows the boundary between safe region and unsafe region, as represented by the sample points.

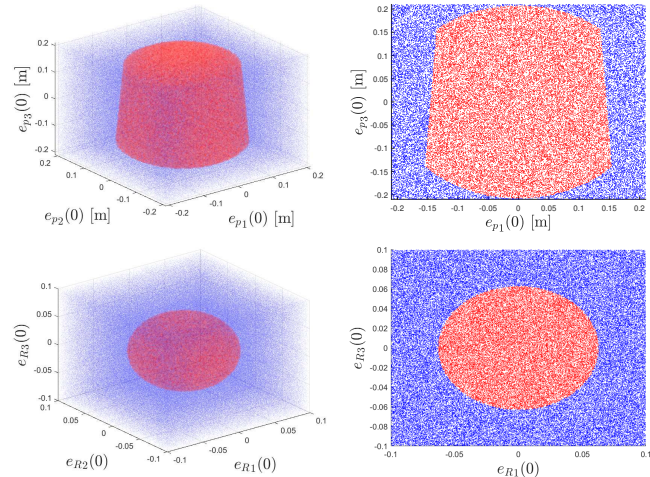


Fig. 4. Sample points approximating the safe initial set characterized by (60) (the red points satisfy (60), whereas the blue points do not satisfy (60)). The top left panel shows a 3D scatter plot of the sample points with position error assuming $e_v(0) = e_R(0) = e_\omega(0) = \mathbf{0}_3$, while the top right panel displays a cross-sectional view when $e_{p2}(0) = 0$. The bottom left panel shows a 3D scatter plot of the sample points with attitude error assuming $e_p(0) = e_v(0) = e_\omega(0) = \mathbf{0}_3$, while the bottom right panel displays a cross-sectional view when $e_{R2}(0) = 0$.

E. Validation of the tracking performance

For the sake of numerical quadrotor simulations, we sample twenty initial points through the following relations: $p(0) = p_d(0) + \text{sample}(0.3[-1_3, 1_3])$, $v(0) = \dot{p}_d(0) + \text{sample}(0.3[-1_3, 1_3])$, $R(0) = e^{(\text{sample}(0.5[-1_3, 1_3]))^\wedge}$, and $\omega(0) = \text{sample}([-1_3, 1_3])$, where only the points satisfying (60) are considered. The generated twenty initial points are adopted to compute trajectories using 4th and 5th order Runge-Kutta methods (RK45 in MATLAB)⁷. The integrated trajectories are depicted in Figure 5. All position profiles associated with the generated trajectories from the chosen twenty points, represented by blue lines, originate from the bottom right corner and terminate at the target set (blue box) located at the top left corner.

To demonstrate the effectiveness of the proposed framework and the safety guarantees for the generated twenty trajectories, the profiles of the functions V , $\|e_p(\cdot)\|$, $\|e_v(\cdot)\|$, v , $\|f(\cdot)\|$, and $F_{d,3}(\cdot)$, are recorded and presented in Figures 6–8. The first subplot of Figure 6 illustrates that the profiles of the function V , associated with the

⁷The standard Runge-Kutta method do not generally preserve the $SO(3)$ structure of the attitude R during numerical integration. However, the Runge-Kutta methods provide convergence guarantees which motivates using them in this section. For structure preserving numerical integration methods, see, e.g., [51].

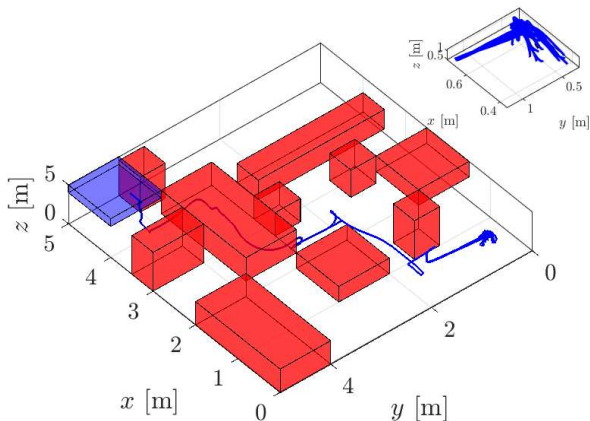


Fig. 5. The generated twenty position trajectories going through the operating domain, avoiding the unsafe set (red boxes) and reaching the target set (blue box). The top right subplot is a zoomed-in view of the trajectories at the initial portion of the simulations.

generated trajectories, are bounded below by $\mathcal{L}_u^2(\bar{\mathcal{V}}_1, \bar{\mathcal{V}}_2)$ for all $t \in [0, T]$, thus validating Corollary 1. The subsequent two subplots of Figure 6 indicate that $\|e_p(\cdot)\|$ and $\|e_v(\cdot)\|$ are bounded by the theoretical bounds $\mathcal{L}_p(\bar{\mathcal{V}}_1, \bar{\mathcal{V}}_2)$ and $\mathcal{L}_v(\bar{\mathcal{V}}_1, \bar{\mathcal{V}}_2)$, respectively, for all $t \in [0, T]$, validating Corollary 2 and illustrating the collision-avoidance and the velocity bound satisfaction for the generated trajectories. In fact, Figure 7 shows clearly how the absolute values of velocity are within $\llbracket 0_3, v_{\max} \rrbracket$, ensuring that the tracking remains within the operational capacity of the quadrotor. The absolute values of the thrust f , shown in the first subplot of Figure 8, are uniformly bounded by $\bar{\mathcal{F}}$, indicating the effectiveness of the thrust bound $\bar{\mathcal{F}}$ and the fulfillment of the requirement of not exceeding f_{\max} . The third component of the desired thrust, $F_{d,3}$, is strictly positive, indicating well-definedness of the closed-loop dynamics for all the generated trajectories (see (22)). The simulations demonstrate that when (60) is fulfilled, the quadrotor performs as expected and the position errors remain perfectly within the theoretical threshold, validating the safety guarantees of the proposed framework.

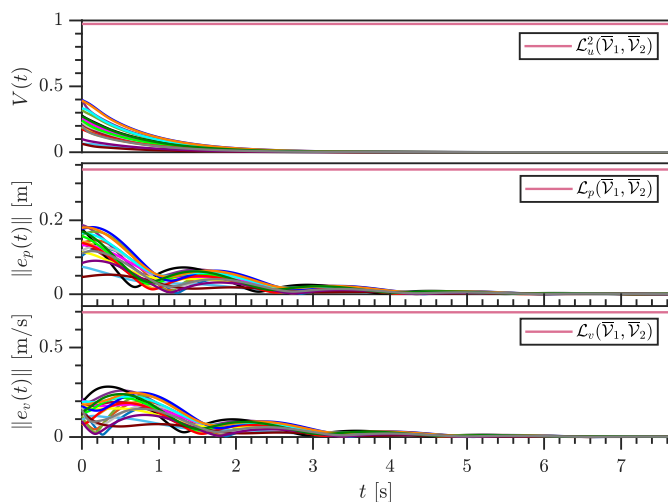


Fig. 6. For all $t \in [0, T]$, $\|e_p\|$, $\|e_v\|$, V remain within the theoretical bounds. Data are only shown for the first 7.7 seconds, however the bounds are still respected for all $t \in [0, T]$.

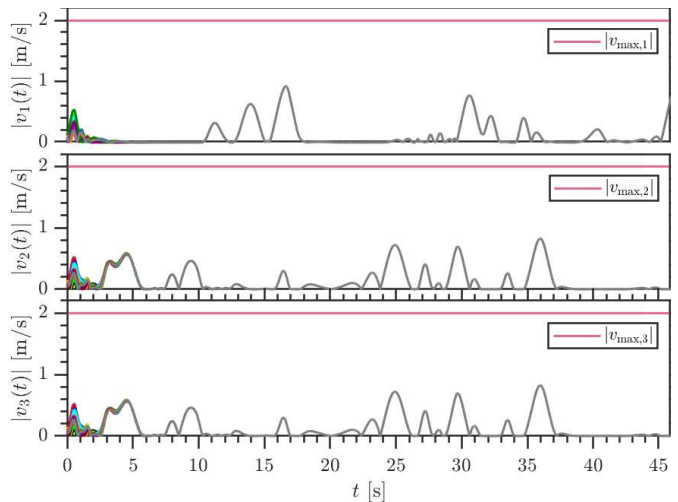


Fig. 7. The three components of $|v|$ all remain within the theoretical bound for all $t \in [0, T]$.

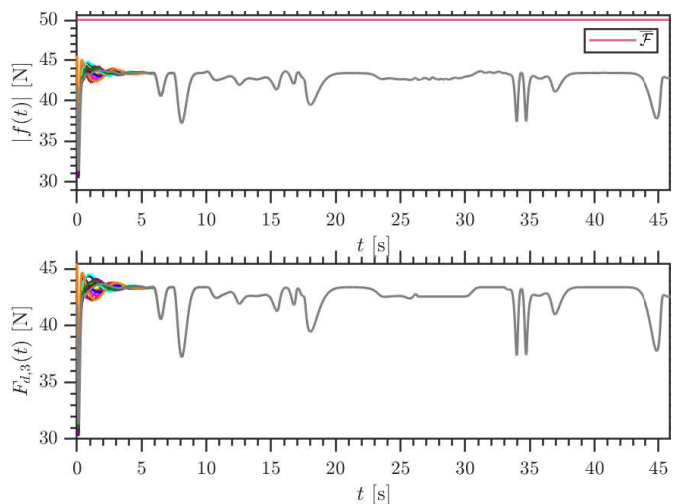


Fig. 8. The profiles of $|f|$ stay within the theoretical bound for all the generated trajectories, where the profiles of $F_{d,3}$ are strictly positive, ensuring well-definedness of the closed-loop dynamics.

IX. CONCLUSION

In this paper, we proposed a control framework for a quadrotor UAV to accomplish reach-avoid tasks with formal safety guarantees, where the standard planning-tracking paradigm is adapted to account for tracking errors. The framework integrates geometric control theory for trajectory tracking and polynomial trajectory generation using Bézier curves, where tracking errors are accounted for during trajectory synthesis. We revisited the stability analysis of the closed-loop quadrotor system under geometric control, where we proved local exponential stability of the tracking error dynamics for any positive control gains and we provided uniform bounds on tracking errors that can be used in planning. We also derived sufficient conditions to be imposed on the desired trajectory to ensure the well-definedness of the closed-loop quadrotor dynamics. The trajectory synthesis involved an efficient algorithm that constructs a safe tube using sampling-based planning and safe hyper-rectangular set computations. The desired trajectory, represented as a piecewise continuous Bézier curve, is computed through the generated safe tube using a heuristic efficient approach, relying on iterative linear programming. Finally, we performed extensive numerical quadrotor simulations to

demonstrate the proposed framework's effectiveness in reach-avoid planning scenarios.

In future work, we plan to incorporate the effects of measurement and input noises and disturbances into the safe planning framework to enable effective real-world applications. Additionally, we aim to extend the proposed control synthesis to cover more complex quadrotor models (e.g., those that account for aerodynamic drag) and more general specifications (e.g., those described by temporal logics). There is also a potential to improve the uniform tracking error bounds in future work by employing modified versions of the geometric tracking control that involve gain matrices instead of scalars, resulting in less conservative trajectory synthesis.

APPENDIX

Proof of Lemma 1

For (a), as M is symmetric, it is diagonalizable, i.e., $M = Q^T D Q$, where $Q \in \mathbb{R}^{n \times n}$ is orthogonal, and $D \in \mathbb{R}^{n \times n}$ is a diagonal matrix whose diagonal entries are the positive eigenvalues of M , $\lambda_1, \dots, \lambda_n$, i.e., $D = \text{diag}([\lambda_1 \cdots \lambda_n]^T)$. Let $y = Qx$. Then,

$$\underline{\lambda}(M) \|y\|^2 \leq x^T M x = y^T D y = \sum_{i=1}^n \lambda_i y_i^2 \leq \bar{\lambda}(M) \|y\|^2.$$

As Q is orthogonal, $\|y\| = \|x\|$, and (a) follows. For (b), first note that as $M \in \mathcal{S}_{++}^n$, its square root $M^{\frac{1}{2}}$ is also in \mathcal{S}_{++}^n . Moreover, $M^{-\frac{1}{2}} \in \mathcal{S}_{++}^n$ and, consequently, $M^{-\frac{1}{2}} W M^{-\frac{1}{2}} \in \mathcal{S}_{++}^n$ (see [30, p. 222]). Therefore, utilizing (a), we have $\|W^{\frac{1}{2}} x\|^2 = x^T W x = x^T M^{\frac{1}{2}} M^{-\frac{1}{2}} W M^{-\frac{1}{2}} M^{\frac{1}{2}} x = (M^{\frac{1}{2}} x)^T (M^{-\frac{1}{2}} W M^{-\frac{1}{2}}) (M^{\frac{1}{2}} x) \geq \underline{\lambda}(M^{-\frac{1}{2}} W M^{-\frac{1}{2}}) \|M^{\frac{1}{2}} x\|^2$. The estimate in (c) follows as $\|A x\| = \|A M^{-\frac{1}{2}} M^{\frac{1}{2}} x\| \leq \|A M^{-\frac{1}{2}}\| \|M^{\frac{1}{2}} x\|$.

Proof of Lemma 6

This follows from Lemma 5, with $b(\cdot) = -(a_0 - a_1 e^{-c(\cdot)})$, and $k(\cdot) = a_2 e^{-c(\cdot)}$. We have

$$\int_0^t b(s) ds = -a_0 t + a_1 \frac{1 - e^{-ct}}{c} \leq -a_0 t + \frac{a_1}{c}, \quad t \in I,$$

which implies $e^{\frac{1}{2} \int_0^t b(s) ds} \leq e^{-\frac{a_0}{2} t} e^{\frac{a_1}{2c}}$. Also, we have

$$-\int_0^t b(s) ds = a_0 t + a_1 \frac{e^{-ct} - 1}{c} \leq a_0 t, \quad t \in I,$$

which yields

$$\int_0^t k(s) e^{-\frac{1}{2} \int_0^s b(z) dz} ds \leq \int_0^t a_2 e^{-cs} e^{\frac{a_0}{2} s} ds, \quad t \in I,$$

and that results in the desired bound.

Proof of Proposition 1

The proof is adapted from [52]. Let $t \in I$. Obviously, $\dot{e}_p(t) = e_v(t)$. The derivative of e_v is given by

$$\begin{aligned} m \dot{e}_v(t) &= m \dot{p}(t) - m \ddot{p}_d(t) = -m g e_3 + f(t) R(t) e_3 - m \ddot{p}_d(t) \\ &= -m g e_3 - m \ddot{p}_d(t) + F_d(t) + (f(t) R(t) e_3 - F_d(t)). \end{aligned}$$

Using the definition of F_d in (17), we have $-m g e_3 - m \ddot{p}_d(t) + F_d(t) = -k_p e_p(t) - k_v e_v(t)$, and $f(t) R(t) e_3 - F_d(t) = (F_d(t) \cdot R(t) e_3) R(t) e_3 - F_d(t) = (\|F_d(t)\| b_{3,d}(t) \cdot b_3(t)) b_3(t) - \|F_d(t)\| b_{3,d}(t) = \|F_d(t)\| ((b_{3,d}(t) \cdot b_3(t)) b_3(t) - b_{3,d}(t)) = \Delta_f(t)$.

Now, we derive the evolution equations for the rotation error dynamics. Let $G: I \rightarrow \text{SO}(3)$ be defined as $G(\cdot) := R_d^T(\cdot) R(\cdot)$.

Note that the rotational error functions can be written in terms of G as follows:

$$\begin{aligned} e_R(\cdot) &= \frac{1}{2} (G(\cdot) + G^T(\cdot))^\vee, \\ e_\omega(\cdot) &= \omega(\cdot) - G^T(\cdot) \omega_d(\cdot), \\ \Psi(\cdot) &= \frac{1}{2} \text{tr}(I_3 - G(\cdot)). \end{aligned}$$

In addition, τ and \mathcal{C} can be written as

$$\begin{aligned} \tau(\cdot) &= -k_R e_R(\cdot) - k_\omega e_\omega(\cdot) + \omega(\cdot) \times J \omega(\cdot) \\ &\quad - J(\dot{\omega}(\cdot) G^T(t) \omega_d(\cdot) - G^T(\cdot) \dot{\omega}_d(\cdot)), \\ \mathcal{C}(\cdot) &= \frac{1}{2} (\text{tr}[G^T(\cdot)] I_3 - G^T(\cdot)). \end{aligned}$$

Using equations (8) and (20), and property (1), the derivative of G is given by

$$\begin{aligned} \dot{G}(t) &= \dot{R}_d^T(t) R(t) + R_d^T(t) \dot{R}(t) \\ &= (R_d(t) \hat{\omega}_d(t))^T R(t) + R_d^T(t) R(t) \hat{\omega}(t) \\ &= -\hat{\omega}_d(t) R_d^T(t) R(t) + R_d^T(t) R(t) \hat{\omega}(t) \\ &= R_d^T(t) R(t) (\hat{\omega}(t) - R^T(t) R_d(t) \hat{\omega}_d(t) R_d^T(t) R(t)) \\ &= G(t) (\hat{\omega}(t) - G^T(t) \hat{\omega}_d(t) G(t)). \end{aligned}$$

Using property (5), we have $G^T(t) \hat{\omega}_d(t) G(t) = (G^T(t) \omega_d(t))^\wedge$. Hence, using the linearity of the hat operator and the definition of e_ω in (14), we have

$$\begin{aligned} \dot{G}(t) &= G(t) (\hat{\omega}(t) - (G^T(t) \omega_d(t))^\wedge) \\ &= G(t) (\omega(t) - G^T(t) \omega_d(t))^\wedge = G(t) \hat{e}_\omega(t). \end{aligned}$$

For the time derivative of Ψ , we have

$$\dot{\Psi}(t) = \frac{1}{2} \text{tr}[0_{3 \times 3} - \dot{G}(t)] = -\frac{1}{2} \text{tr}[G(t) \hat{e}_\omega(t)].$$

Using property (3) and the definition of e_R , we have

$$\dot{\Psi}(t) = \frac{1}{2} e_\omega^T(t) (G(t) - G^T(t))^\wedge = e_\omega^T(t) e_R(t) = e_\omega(t) \cdot e_R(t).$$

For the time derivative of e_R , we have, where we use properties (1) and (4),

$$\begin{aligned} \dot{e}_R(t) &= \frac{1}{2} (\dot{G}(t) - \dot{G}^T(t))^\vee = \frac{1}{2} (G(t) \hat{e}_\omega(t) - \hat{e}_\omega^T(t) G^T(t))^\vee \\ &= \frac{1}{2} (G(t) \hat{e}_\omega(t) + \hat{e}_\omega(t) G^T(t))^\vee \\ &= \frac{1}{2} (\text{tr}[G^T(t)] I_3 - G^T(t)) e_\omega(t) = \mathcal{C}(t) e_\omega(t). \end{aligned}$$

For the time derivative of e_ω , noting that $e_\omega(t) = \omega(t) - G^T(t) \omega_d(t)$, we have

$$\begin{aligned} \dot{e}_\omega(t) &= \dot{\omega}(t) - \dot{G}^T(t) \omega_d(t) - G^T(t) \dot{\omega}_d(t) \\ &= \dot{\omega}(t) - \hat{e}_\omega^T(t) G^T(t) \omega_d(t) - G^T(t) \dot{\omega}_d(t) \\ &= \dot{\omega}(t) + \hat{e}_\omega(t) G^T(t) \omega_d(t) - G^T(t) \dot{\omega}_d(t). \end{aligned}$$

Substituting equation (9) in yields

$$\begin{aligned} \dot{e}_\omega(t) &= J^{-1} (-\omega(t) \times J \omega(t) + \tau(t)) \\ &\quad + \hat{e}_\omega(t) G^T(t) \omega_d(t) - G^T(t) \dot{\omega}_d(t). \end{aligned}$$

Substituting the expression of τ in the formula of \dot{e}_ω yields

$$\begin{aligned} \dot{e}_\omega(t) &= J^{-1} (-k_R e_R(t) - k_\omega e_\omega(t)) \\ &\quad - \hat{\omega}(t) G^T(t) \omega_d(t) + \hat{e}_\omega(t) G^T(t) \omega_d(t). \end{aligned}$$

Note that, using the linearity of the hat operator and property (5), we have $\hat{e}_\omega(t) = (\omega(t) - G^T(t) \omega_d(t))^\wedge = \hat{\omega}(t) - (G^T(t) \omega_d(t))^\wedge =$

$\hat{\omega}(t) - G^\top(t)\hat{\omega}_d(t)G(t)$. Hence,

$$\begin{aligned} & -\hat{\omega}(t)G^\top(t)\omega_d(t) + \hat{e}_\omega(t)G^\top(t)\omega_d(t) \\ & = -G^\top(t)\hat{\omega}_d(t)G(t)G^\top(t)\omega_d(t) \\ & = -G^\top(t)\hat{\omega}_d(t)\omega_d(t) = 0_3 \end{aligned}$$

as $\hat{\omega}_d(t)\omega_d(t) = \omega_d(t) \times \omega_d(t) = 0_3$, and that completes the proof.

Proof of Lemma 8

This proof is adapted from [39]. Using Lemma 3, let $x \in \mathbb{R}^3$ be such that $A = R^\top(t)R_d(t) = \exp(\hat{x})$ (assume without loss of generality that $x \neq 0_3$). Then, it can be shown that $\text{tr}(A) = 1 + 2\cos(\|x\|)$ and that $\frac{A+A^\top}{2}$ has the eigenvalues 1 and $\cos(\|x\|)$ (repeated). In addition, $C^\top(t)C(t)$ can be written as

$$C^\top(t)C(t) = \frac{1}{4} \left((\text{tr}^2(A) + 1)\mathbf{I}_3 - 2\text{tr}(A)\left(\frac{A+A^\top}{2}\right) \right).$$

This indicates that the eigenvalues of $C^\top(t)C(t)$ are

$$\begin{aligned} \lambda_1(C^\top(t)C(t)) &= \frac{1}{4} \left((1 + 2\cos(\|x\|))^2 + 1 - 2(1 + 2\cos(\|x\|)) \right) \\ &= \cos^2(\|x\|) \end{aligned}$$

and

$$\begin{aligned} \lambda_2(C^\top(t)C(t)) &= \frac{1}{4} (1 + 2\cos(\|x\|))^2 \\ &+ \frac{1}{4} (1 - 2(1 + 2\cos(\|x\|)) \cos(\|x\|)) \\ &= \frac{1 + \cos(\|x\|)}{2} \text{ (repeated),} \end{aligned}$$

which are less than or equal to one, and that completes the proof.

Proof of Lemma 9

The proof is adapted from [39]. Using Lemma 3, let $x \in \mathbb{R}^3$ such that $R_d^\top(t)R(t) = \exp(\hat{x})$ (without loss of generality, assume $x \neq 0_3$). Then, we have $\Psi(t) = 1 - \cos(\|x\|)$, and $e_R(t) = \sin(\|x\|)x/\|x\|$, implying $\|e_R(t)\|^2 = \sin^2(\|x\|)$. It then follows that $0 \leq \Psi(t) \leq 2$, $\|e_R(t)\| \leq 1$, and $\|e_R(t)\|^2 = \sin^2(\|x\|) = 1 - \cos^2(\|x\|) = (1 - \cos(\|x\|))(1 + \cos(\|x\|)) = (1 - \cos(\|x\|))(2 - (1 - \cos(\|x\|))) = \Psi(t)(2 - \Psi(t))$. Assume without loss of generality that $\|x\| \neq (2n+1)\pi$, $n \in \mathbb{Z}_+$, then $\|e_R(t)\|^2/2 \leq \|e_R(t)\|^2/(2 - \Psi(t)) = \Psi(t)$. With the assumption that $\Psi(t) \leq \psi < 2$, we have $\Psi(t) = \|e_R(t)\|^2/(2 - \Psi(t)) \leq \|e_R(t)\|^2/(2 - \psi)$.

Proof of Lemma 10

Let $A = R_d^\top(t)R(t)$. We have $\|(b_{3,d}(t) \cdot b_3(t))b_3(t) - b_{3,d}(t)\|^2 = (b_{3,d}(t) \cdot b_3(t))^2 b_3(t) \cdot b_3(t) - 2(b_{3,d}(t) \cdot b_3(t))^2 + b_{3,d}(t) \cdot b_{3,d}(t) = 1 - ((b_{3,d}(t) \cdot b_3(t))^2) = 1 - (A_{3,3})^2$. Using Lemma 3, let $x \in \mathbb{R}^3$ such that $A = \exp(\hat{x})$ (without loss of generality, assume $x \neq 0_3$). As we showed in the proof of Lemma 9, we have $\|e_R(t)\|^2 = \sin^2(\|x\|)$ and $\Psi(t) = 1 - \cos(\|x\|)$. The expression of $1 - (A_{3,3})^2$ is given as

$$1 - A_{3,3}^2 = 1 - \left(1 + \frac{(x_1^2 + x_2^2)(\cos(\|x\|) - 1)}{\|x\|^2} \right)^2.$$

Let $\alpha_x := (x_1^2 + x_2^2)/\|x\|^2$. Note that $0 \leq \alpha_x \leq 1$. The term $1 - (A_{3,3})^2$ can then be rewritten as $1 - (A_{3,3})^2 = 1 - (1 - \alpha_x \Psi(t))^2 = \alpha_x \Psi(t)(2 - \alpha_x \Psi(t))$. As $0 \leq \Psi(t) \leq \psi < 2$ and $0 \leq \alpha_x \leq 1$, we have, using Lemma 9, $\alpha_x \Psi(t)(2 - \alpha_x \Psi(t)) \leq 2\alpha_x \Psi(t) \leq 2\Psi(t) \leq \frac{2}{2-\psi} \|e_R(t)\|^2$.

Proof of Lemma 14

We have $e_p(0) = e_v(0) = 0_3$. Consequently, and using the definition of R_d in (19) and fact that $\ddot{p}_d(0) = 0_3$, we have $R_d(0) = R(0) = \mathbf{I}_3$. Finally, we note that

$$\dot{F}_d(t) = -k_p e_v(t) - \frac{k_v}{m} (-k_p e_p(t) - k_v e_v(t) + \Delta_f(t)) + \ddot{p}_d(t), \quad (82)$$

$t \in I$. As $R(0) = R_d(0)$, we have $\Delta_f(0) = 0$, and with the assumption on $\ddot{p}_d(0)$, we have $\dot{F}_d(0) = 0_3$, implying $\dot{R}_d(0) = 0_{3 \times 3}$. Finally, using the definition of ω_d in (14), the proof is complete.

Proof of Lemma 15

The proof is taken from [48]. For any $z \in \mathbb{R}^n$, with $|z - v| \leq r$, $|z - \text{center}(\llbracket a, b \rrbracket)| \leq |z - v| + |v - \text{center}(\llbracket a, b \rrbracket)| \leq \text{radius}(\llbracket a, b \rrbracket) - |\text{center}(\llbracket a, b \rrbracket) - v| + |\text{center}(\llbracket a, b \rrbracket) - v| = \text{radius}(\llbracket a, b \rrbracket)$.

Proof of Lemma 16

The proof is taken from [48]. The first claim follows by noting that, for all $y \in \llbracket a, b \rrbracket$, $|x_i - y_i^*| \leq |x_i - y_i|$, $i \in [1; n]$. For the second claim, let $z \in \mathcal{S}(x, \llbracket a, b \rrbracket, \alpha)$, then $|z_{\bar{i}} - x_{\bar{i}}| \leq \alpha \|x - y^*\|_\infty < \|x - y^*\|_\infty$. Assume, without loss of generality, that $x_{\bar{i}} \geq c_{\bar{i}}$, then it holds, using the definition and minimal property of y^* , that $x_{\bar{i}} - c_{\bar{i}} \geq \|x - y^*\|_\infty + r_{\bar{i}}$. Consequently, $z_{\bar{i}} - c_{\bar{i}} = z_{\bar{i}} - x_{\bar{i}} + x_{\bar{i}} - c_{\bar{i}} \geq -|z_{\bar{i}} - x_{\bar{i}}| + \|x - y^*\|_\infty + r_{\bar{i}} > -\|x - y^*\|_\infty + \|x - y^*\|_\infty + r_{\bar{i}} = r_{\bar{i}}$. Hence, $|z_{\bar{i}} - c_{\bar{i}}| > r_{\bar{i}}$, implying $z \notin \llbracket a, b \rrbracket$.

REFERENCES

- [1] S. M. Raafat, F. A. Raheem, A. A. Alawsi, and Z. S. Mahmood, *Application and Control of Quadrotors*, pp. 241–264. Cham: Springer International Publishing, 2022.
- [2] D. Mellinger and V. Kumar, “Minimum snap trajectory generation and control for quadrotors,” in *2011 IEEE international conference on robotics and automation*, pp. 2520–2525, IEEE, 2011.
- [3] C. Richter, A. Bry, and N. Roy, “Polynomial trajectory planning for aggressive quadrotor flight in dense indoor environments,” in *Robotics Research: The 16th International Symposium ISRR*, pp. 649–666, Springer, 2016.
- [4] G. Farid, S. Cocuzza, T. Younas, A. A. Razzaqi, W. A. Wattoo, F. Cannella, and H. Mo, “Modified A-star (A*) approach to plan the motion of a quadrotor UAV in three-dimensional obstacle-cluttered environment,” *Applied Sciences*, vol. 12, no. 12, p. 5791, 2022.
- [5] Y. V. Pant, H. Abbas, R. A. Quayy, and R. Mangharam, “Fly-by-logic: Control of multi-drone fleets with temporal logic objectives,” in *2018 ACM/IEEE 9th International Conference on Cyber-Physical Systems (ICCPs)*, pp. 186–197, IEEE, 2018.
- [6] F. Gao, W. Wu, Y. Lin, and S. Shen, “Online safe trajectory generation for quadrotors using fast marching method and bernstein basis polynomial,” in *2018 IEEE International Conference on Robotics and Automation (ICRA)*, pp. 344–351, IEEE, 2018.
- [7] G. Hoffmann, S. Waslander, and C. Tomlin, “Quadrotor helicopter trajectory tracking control,” in *AIAA guidance, navigation and control conference and exhibit*, p. 7410, 2008.
- [8] E. C. Suicmez and A. T. Kutay, “Optimal path tracking control of a quadrotor UAV,” in *2014 International Conference on Unmanned Aircraft Systems (ICUAS)*, pp. 115–125, IEEE, 2014.
- [9] S.-h. Lee, S. H. Kang, and Y. Kim, “Trajectory tracking control of quadrotor UAV,” in *2011 11th International Conference on Control, Automation and Systems*, pp. 281–285, IEEE, 2011.
- [10] D. E. Chang and Y. Eun, “Global chartwise feedback linearization of the quadcopter with a thrust positivity preserving dynamic extension,” *IEEE Transactions on Automatic Control*, vol. 62, no. 9, pp. 4747–4752, 2017.
- [11] S. Bouabdallah and R. Siegwart, “Backstepping and sliding-mode techniques applied to an indoor micro quadrotor,” in *Proceedings of the 2005 IEEE international conference on robotics and automation*, pp. 2247–2252, IEEE, 2005.

- [12] C. Liu, H. Lu, and W.-H. Chen, "An explicit MPC for quadrotor trajectory tracking," in *2015 34th Chinese Control Conference (CCC)*, pp. 4055–4060, IEEE, 2015.
- [13] A. Andri n, E. Lefeber, D. Antunes, and W. Heemels, "Model predictive control for quadcopters with almost global trajectory tracking guarantees," *IEEE Transactions on Automatic Control*, 2024.
- [14] E. Lefeber, S. Van den Eijnden, and H. Nijmeijer, "Almost global tracking control of a quadrotor UAV on SE(3)," in *2017 IEEE 56th Annual Conference on Decision and Control (CDC)*, pp. 1175–1180, IEEE, 2017.
- [15] T. Lee, M. Leok, and N. H. McClamroch, "Geometric tracking control of a quadrotor UAV on SE(3)," in *49th IEEE conference on decision and control (CDC)*, pp. 5420–5425, IEEE, 2010.
- [16] R. Amin, L. Aijun, and S. Shamshirband, "A review of quadrotor UAV: control methodologies and performance evaluation," *International Journal of Automation and Control*, vol. 10, no. 2, pp. 87–103, 2016.
- [17] G. Reissig, A. Weber, and M. Rungger, "Feedback refinement relations for the synthesis of symbolic controllers," *IEEE Transactions on Automatic Control*, vol. 62, no. 4, pp. 1781–1796, 2016.
- [18] M. Zamani, G. Pola, M. Mazo, and P. Tabuada, "Symbolic models for nonlinear control systems without stability assumptions," *IEEE Transactions on Automatic Control*, vol. 57, no. 7, pp. 1804–1809, 2011.
- [19] J. Liu and N. Ozay, "Abstraction, discretization, and robustness in temporal logic control of dynamical systems," in *Proceedings of the 17th international conference on Hybrid systems: computation and control*, pp. 293–302, 2014.
- [20] Y. Li and J. Liu, *Formal Methods for Control of Nonlinear Systems*. Chapman and Hall/CRC, 2022.
- [21] I. R. Manchester and J.-J. E. Slotine, "Control contraction metrics: Convex and intrinsic criteria for nonlinear feedback design," *IEEE Transactions on Automatic Control*, vol. 62, no. 6, pp. 3046–3053, 2017.
- [22] P. Zhao, A. Lakshmanan, K. Ackerman, A. Gahlawat, M. Pavone, and N. Hovakimyan, "Tube-certified trajectory tracking for nonlinear systems with robust control contraction metrics," *IEEE Robotics and Automation Letters*, vol. 7, no. 2, pp. 5528–5535, 2022.
- [23] S. Singh, B. Landry, A. Majumdar, J.-J. Slotine, and M. Pavone, "Robust feedback motion planning via contraction theory," *The International Journal of Robotics Research*, vol. 42, no. 9, pp. 655–688, 2023.
- [24] A. Saffi, M. N. Zeilinger, and J. K hler, "Robust adaptive MPC using control contraction metrics," *Automatica*, vol. 155, p. 111169, 2023.
- [25] A. D. Ames, S. Coogan, M. Egerstedt, G. Notomista, K. Sreenath, and P. Tabuada, "Control barrier functions: Theory and applications," in *2019 18th European control conference (ECC)*, pp. 3420–3431, IEEE, 2019.
- [26] M. Khan, M. Zafar, and A. Chatterjee, "Barrier functions in cascaded controller: Safe quadrotor control," in *2020 American Control Conference (ACC)*, pp. 1737–1742, IEEE, 2020.
- [27] T. Lee, "Global exponential attitude tracking controls on SO(3)," *IEEE Transactions on Automatic Control*, vol. 60, no. 10, pp. 2837–2842, 2015.
- [28] T. Fernando, J. Chandiramani, T. Lee, and H. Gutierrez, "Robust adaptive geometric tracking controls on SO(3) with an application to the attitude dynamics of a quadrotor UAV," in *2011 50th IEEE conference on decision and control and European control conference*, pp. 7380–7385, IEEE, 2011.
- [29] I. Kolmanovskiy, E. G. Gilbert, *et al.*, "Theory and computation of disturbance invariant sets for discrete-time linear systems," *Mathematical problems in engineering*, vol. 4, pp. 317–367, 1998.
- [30] K. M. Abadir and J. R. Magnus, *Matrix Algebra*. Econometric Exercises, Cambridge University Press, 2005.
- [31] R. A. Horn and C. R. Johnson, *Matrix analysis*. Cambridge university press, 2 ed., 2012.
- [32] B. C. Hall and B. C. Hall, *Lie groups, Lie algebras, and representations*. Springer, 2013.
- [33] J. Gallier and D. Xu, "Computing exponentials of skew-symmetric matrices and logarithms of orthogonal matrices," *International Journal of Robotics and Automation*, vol. 18, no. 1, pp. 10–20, 2003.
- [34] J. S. Dai, "Euler–rod rigues formula variations, quaternion conjugation and intrinsic connections," *Mechanism and Machine Theory*, vol. 92, pp. 144–152, 2015.
- [35] D. D. Bainov and P. S. Simeonov, *Integral inequalities and applications*, vol. 57. Springer Science & Business Media, 2013.
- [36] R. T. Farouki, *Pythagorean–Hodograph Curves*. Springer, 2008.
- [37] G. Farin, *Curves and surfaces for computer-aided geometric design: a practical guide*. Elsevier, 2014.
- [38] M. Y. Vardi, "An automata-theoretic approach to linear temporal logic," *Logics for concurrency: structure versus automata*, pp. 238–266, 2005.
- [39] T. Lee, M. Leok, and N. H. McClamroch, "Control of complex maneuvers for a quadrotor UAV using geometric methods on SE(3)," *arXiv preprint arXiv:1003.2005*, 2010.
- [40] Y. Zou, "Trajectory tracking controller for quadrotors without velocity and angular velocity measurements," *IET Control Theory & Applications*, vol. 11, no. 1, pp. 101–109, 2017.
- [41] F. Zhang, *The Schur complement and its applications*, vol. 4. Springer Science & Business Media, 2006.
- [42] S. Sastry, *Nonlinear systems: analysis, stability, and control*, vol. 10. Springer Science & Business Media, 2013.
- [43] G. David, C. Schaeffer, and W. John, *Ordinary differential equations: Basics and beyond*. Springer, 2018.
- [44] H. Logemann, E. P. Ryan, *et al.*, *Ordinary differential equations: analysis, qualitative theory and control*. Springer, 2014.
- [45] Q. Kong, *A short course in ordinary differential equations*. Springer, 2014.
- [46] T. Marcucci, M. Petersen, D. von Wrangel, and R. Tedrake, "Motion planning around obstacles with convex optimization," *Science robotics*, vol. 8, no. 84, p. eadf7843, 2023.
- [47] L. E. Kavraki, P. Svestka, J.-C. Latombe, and M. H. Overmars, "Probabilistic roadmaps for path planning in high-dimensional configuration spaces," *IEEE transactions on Robotics and Automation*, vol. 12, no. 4, pp. 566–580, 1996.
- [48] M. Serry, L. Yang, N. Ozay, and J. Liu, "Safe tracking control of discrete-time nonlinear systems using backward reachable sets," in *2024 American Control Conference (ACC) (Accepted)*, IEEE, 2024.
- [49] Oliver, "PLOTcube." MATLAB Central File Exchange: <https://www.mathworks.com/matlabcentral/fileexchange/15161-2024>. [Online; accessed May, 2024].
- [50] S. Kirkpatrick, C. D. Gelatt Jr, and M. P. Vecchi, "Optimization by simulated annealing," *science*, vol. 220, no. 4598, pp. 671–680, 1983.
- [51] E. Hairer, M. Hochbruck, A. Iserles, and C. Lubich, "Geometric numerical integration," *Oberwolfach Reports*, vol. 3, no. 1, pp. 805–882, 2006.
- [52] T. Lee, "Robust adaptive attitude tracking on SO(3) with an application to a quadrotor UAV," *IEEE Transactions on Control Systems Technology*, vol. 21, no. 5, pp. 1924–1930, 2012.